Geophys. J. Int. (2009) **179,** 579–600 doi: 10.1111/j.1365-246X.2009.04298.x

Deep lithospheric structures along the southern central Chile margin from wide-angle *P*-wave modelling

M. Scherwath, E. Contreras-Reyes,* E. R. Flueh, I. Grevemeyer, A. Krabbenhoeft, C. Papenberg, C. J. Petersen† and R. W. Weinrebe

Leibniz Institute of Marine Sciences, IFM-GEOMAR, Wischhofstr. 1-3, 24148 *Kiel, Germany. E-mail: mscherwath@ifm-geomar.de*

Accepted 2009 June 15. Received 2009 June 15; in original form 2008 August 8

SUMMARY

Crustal- and upper-mantle structures of the subduction zone in south central Chile, between 42°S and 46°S, are determined from seismic wide-angle reflection and refraction data, using the seismic ray tracing method to calculate minimum parameter models. Three profiles along differently aged segments of the subducting Nazca Plate were analysed in order to study subduction zone structure dependencies related to the age, that is, thermal state, of the incoming plate. The age of the oceanic crust at the trench ranges from 3 Ma on the southernmost profile, immediately north of the Chile triple junction, to 6.5 Ma old about 100 km to the north, and to 14.5 Ma old another 200 km further north, off the Island of Chiloe. Remarkable similarities appear in the structures of both the incoming as well as the overriding plate. The oceanic Nazca Plate is around 5 km thick, with a slightly increasing thickness northward, reflecting temperature changes at the time of crustal generation. The trench basin is about 2 km thick except in the south where the Chile Ridge is close to the deformation front and only a small, 800-m-thick trench infill could develop. In south central Chile, typically three quarters (1.5 km) of the trench sediments subduct below the decollement in the subduction channel. To the north and south of the study area, only about one quarter to one third of the sediments subducts, the rest is accreted above. Similarities in the overriding plate are the width of the active accretionary prism, 35–50 km, and a strong lateral crustal velocity gradient zone about 75–80 km landward from the deformation front, where landward upper-crustal velocities of over 5.0–5.4 km s^{-1} decrease seaward to around 4.5 km s^{-1} within about 10 km, which possibly represents a palaeo-backstop. This zone is also accompanied by strong intraplate seismicity. Differences in the subduction zone structures exist in the outer rise region, where the northern profile exhibits a clear bulge of uplifted oceanic lithosphere prior to subduction whereas the younger structures have a less developed outer rise. This plate bending is accompanied by strongly reduced rock velocities on the northern profile due to fracturing and possible hydration of the crust and upper mantle. The southern profiles do not exhibit such a strong alteration of the lithosphere, although this effect may be counteracted by plate cooling effects, which are reflected in increasing rock velocities away from the spreading centre. Overall there appears little influence of incoming plate age on the subduction zone structure which may explain why the $M_w = 9.5$ great Chile earthquake from 1960 ruptured through all these differing age segments. The rupture area, however, appears to coincide with a relatively thick subduction channel.

Key words: Controlled source seismology; Seismic tomography; Subduction zone processes; Continental margins: convergent; Crustal structure; South America.

1 INTRODUCTION

South central Chile represents one of the most favourable natural laboratories to study subduction zone processes and their dependence on age, that is, the influence of the thermal state of the incoming plate on subduction zone processes. At 46.5°S the

*Now at: Departamento de Geofísica, Universidad de Chile, Blanco Encalada 2002, Santiago de Chile, Chile.
†Now at: RWE Dea AG, Ueberseering 40, 22297 Hamburg, Germany.

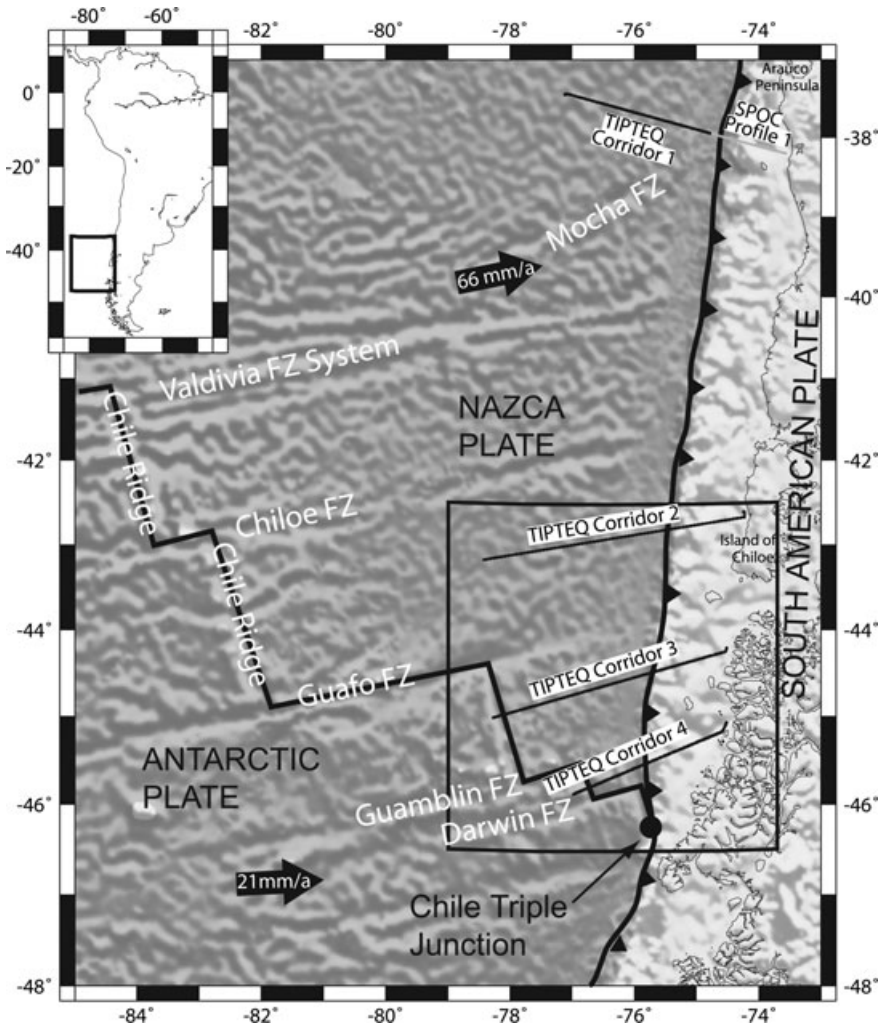

Figure 1. Overview map offshore south central Chile. Inset shows location of working area with respect to South America. Main map shows illuminated bathymetry. Oceanic plates are in dark grey. The actively spreading Chile Ridge is offset by several fracture zones (FZ) and separates the Nazca and Antarctic Plates. Light grey marks overriding continental South American Plate. All three tectonic plates join at the Chile triple junction, marked as black circle. Plate motion vectors relative to South American Plate show convergence rate (DeMets *et al.* 1994; Angermann *et al.* 1999). Major data corridors of TIPTEQ project are also shown, with area of Fig. 2 drawn as large black square.

actively spreading Chile Ridge enters the Chile margin and submerges beneath the continental South American Plate at the Chile triple junction (Fig. 1). Within 1000 km to the north of the Chile triple junction, the age of the incoming Nazca Plate increases from 0 to 30 Myr, and several cross-cutting fracture zones divide the young oceanic plate into distinct segments of thermally quite different subducting lithosphere (Cande & Leslie 1986; Tebbens *et al.* 1997). This paper focuses on the structure of the incoming and overriding plates at the southern central Chile margin along three distinct sections with different age of the subducting plate to investigate possible dependencies of plate age and thus temperature.

The importance of temperature at the subduction interface lies mainly in the seismicity because the seismogenic zone appears strongly dependent on the temperature distribution (Hyndman & Wang 1993; Oleskevich *et al.* 1999; Currie *et al.* 2002). In particular, the subduction of young lithosphere, where the temperature range for thrust earthquakes exists in the shallow, flat part, is often accompanied by large mega-thrust earthquakes. The largest earthquake ever recorded, the $M_w = 9.5$ event of 1960, happened in our working area in the south central Chile region (Cifuentes 1989; Barrientos & Ward 1990). For oceanic lithosphere, the most pronounced changes occur in the first 20 Myr, when the strongest change in thermal state and earthquake depths are observed (Kirby *et al.* 1996; Stein & Stein 1996).

Our study is part of the TIPTEQ project (from The Incoming Plate to mega-Thrust EarthQuake processes) with the objectives to investigate the structure and thermal state of the oceanic plate and the subduction zone, the composition and rheology of the subducting sediment, seismicity and nucleation of large subduction-related earthquakes, and the role of water in all of the above (Rietbrock *et al.* 2005; Scherwath *et al.* 2006). TIPTEQ therefore comprises active and passive source seismology on- and offshore for structure and seismicity information (Haberland *et al.* 2006; Scherwath *et al.* 2006; Contreras-Reyes *et al.* 2007, 2008a,b; Lange *et al.* 2007; Gross *et al.* 2008; Tilmann *et al.* 2008), heat-flow measurements for thermal modelling (Voelker *et al.* 2007; Heesemann *et al.* 2007), sediment probing for compositional, chemical and mechanical data (Roeser *et al.* 2007), magnetotelluric soundings for subsurface resistivity (Kapinos & Brasse 2006; Brasse *et al.* 2009), and extensive

multibeam bathymetric mapping throughout the entire survey area offshore (Scherwath *et al.* 2006).

Other areas with relatively young subducting oceanic plate are Cascadia (e.g. Hyndman & Wang 1993) and Central America (e.g. Currie *et al.* 2002), though none of these have been systematically studied for the variation in age of the incoming plate. Therefore, the TIPTEQ project presents a unique opportunity for the study of subduction zone processes where an incoming plate of younger ages is involved.

In this paper, results from seismic wide-angle reflection and refraction data are presented. The structure and deformation of both the incoming oceanic Nazca Plate and the overriding continental South American Plate are shown.

2 TECTONIC SETTING

In south central Chile, the incoming oceanic lithosphere of the subduction zone comprises both the Nazca Plate to the north and the Antarctic Plate to the south of the Chile Ridge (Fig. 1). The Chile Ridge encounters the overriding, continental South American Plate to form the Chile Triple Junction at 46.5°S (Fig. 1). The half spreading rate at the Chile Ridge has been 31 mm a^{-1} since 5 Ma, but back to 25 Ma varied between 38 and 61 mm a^{-1} (Tebbens *et al.* 1997). The spreading centre is actively subducting south of the Chile Tripe Junction. North of the triple junction the Nazca Plate subducts beneath the South American Plate at a rate of 66 mm/a directed at N80°E (DeMets *et al.* 1994; Angermann *et al.* 1999). The Chile Margin strikes around N95°E, thus the plate convergence in this region is 15°.

Active spreading at the Chile Ridge implies that the subducting lithosphere is young. The age of the Nazca Plate directly at the Chile Margin ranges from 0 at the triple junction to about 30 Myr offshore the Arauco peninsula, the northern limit of our working area offshore (Fig. 1). Several fracture zones divide the Nazca Plate into segments of distinct ages at the trench (Fig. 1).

The composition of the overriding part of the South American Plate is divided into the Coastal Platform (Cenozoic marine and continental sediments), the Coastal Cordillera (crystalline basement of Palaeozoic accretionary complex and magmatic arc), the Central Depression (Pliocene–Quaternary sediment filled basin), and finally the Main Cordillera (active volcanic arc) (Melnick *et al.* 2006).

Along the Chile Margin, the subduction style changes from being erosional north of the Juan Fernandez Ridge (33°S) to accretionary in the south, though with the exception of the Chile Ridge subduction which erodes the overriding plate (Bangs & Cande 1997; Ranero *et al.* 2006). Because of episodes of small sediment supply in our study area basal erosion of both the upper plate and especially any former accretionary structures occurred, and so a reconstruction of the convergence history within the sediments was rendered impossible (Bangs & Cande 1997). The analysis of forearc basin structures suggests that the change from subduction erosion to accretion occurred about 3 Ma ago (Melnick & Echtler 2006). According to the size of the accretionary wedge, accretion has been active for the last 1–2 Myr, but a large part of the incoming sediment is actively subducting (Bangs & Cande 1997; Diaz-Naveas 1999; Behrmann & Kopf 2001; Ranero *et al.* 2006).

Seismologically, south central Chile represents one of the most active regions on the planet, with large to giant mega-thrust earthquakes occurring every 130 and 300 yr, respectively (Cisternas *et al.* 2005). The largest historic earthquake, occurring in 1960 with a magnitude of $M_w = 9.5$, ruptured over a length of almost 1000 km from 37°S down to 46°S near the Chile junction (Cifuentes 1989; Barrientos & Ward 1990). We concentrated our efforts on the southern part of this area, where this giant earthquake ruptured across several segments of differing age of subducting lithosphere.

3 SEISMIC DATA

The data analysis focuses on the structures along the TIPTEQ Corridors 3 and 4 (Fig. 2). Both extend from the spreading centre at the Chile Ridge onto the continental shelf up to a few kilometres off the coast, resulting in lengths of 320 and 225 km for Corridors 3 and 4, respectively. In addition, TIPTEQ Corridor 2 (Fig. 2), where the oceanic part has been analysed and published by Contreras-Reyes *et al.* (2007), was extended up the continental shelf and the results are also shown here. This corridor has a total length of 350 km, though only the easternmost 75 km are analysed here.

Ocean bottom seismometers (Bialas & Flueh 1999) and hydrophones (Flueh & Bialas 1996), hereinafter referred to as OBS/H, were placed along the corridors at a nominal spacing of 5.5 km. The seismic source was a 64-l (3900 cubic inch) airgun array fired about every 100–150 m. In addition, a short 16-channel streamer was towed behind the vessel during the wide-angle data acquisition to provide some constraints on the shallow structures.

Of the 50 OBS/H of Corridor 3, 45 stations were of sufficient quality for subsequent data analysis, and 34 out of 37 OBS/H of Corridor 4 could be used. The data quality of these profiles was limited by relatively high attenuation due to the young age of the plate and the rough basement topography, and so the seismic signals could only be identified up to offsets of 100 km. On Corridor 2, previously 28 OBS/H stations on the oceanic plate and three stations on the shelf were modelled (Contreras-Reyes *et al.* 2007), and here we incorporated the remaining six stations on the shelf and two seismological stations on land (Lange *et al.* 2007) for completion. This northern profile exhibits better data quality than the southern two profiles (see Section 5.2 for data examples).

Additional information on the shallow structures and the decollement reflector in particular is available from seismic multichannel data collected in 1988 by the Lamont Dohorty Earth Observatory, cruise RC 2901 of the RV Conrad (e.g. Bangs & Cande 1997), processed in a basic conventional manner up to finite difference migration. Two of these seismic lines are nearly coincident with TIPTEQ Corridors 3 and 4, respectively, but are oriented at a slightly different angle. To compensate for the slight difference in shallow structures between the TIPTEQ lines and the RV Conrad lines, a small static time-shift was calculated taking into account the differences in water depths.

4 WIDE-ANGLE DATA MODELLING

4.1 Method

We utilise the ray-tracing method of Zelt & Smith (1992) for determining a structural model that matches the observed seismic data. The method performs forward ray tracing through a suitably parameterised model of depth interfaces and velocity nodes to determine the mismatch between measured and predicted arrival times of the measured phases. This mismatch in the form of travel time residuals can be used either to calculate changes in model depth- and velocity-nodes automatically during a linear inversion in a least-square sense, or the model can be adjusted manually to accommodate the data misfit. If applying the inversion, an automatically

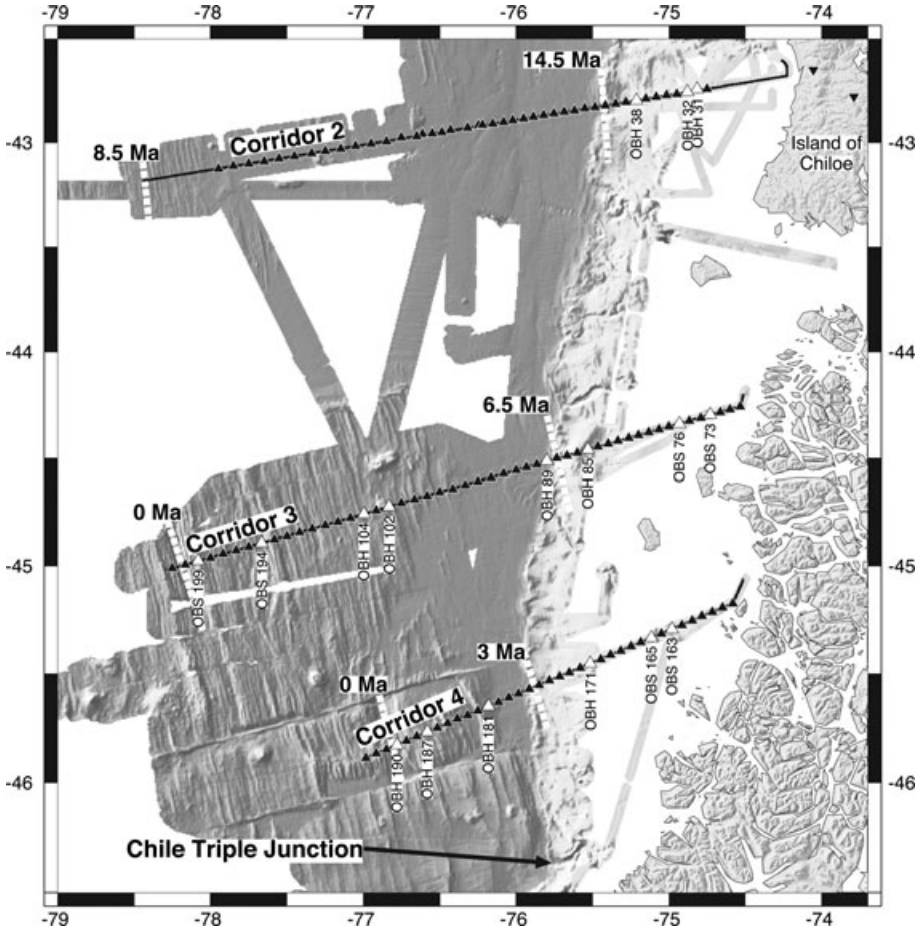

Figure 2. Basemap of the three TIPTEQ seismic profiles analysed in this paper. High resolution bathymetry from TIPTEQ cruise SO181 and from Bourgois *et al.* (2000). Small black triangles represent locations of ocean bottom seismic instruments and the black lines are ship tracks during seismic shooting. Also shown is the age of the incoming oceanic plate near the western end of the profiles and at the intersection of the profiles with the trench. Highlighted are selected stations for data examples discussed in Section 5.2 and in the Supporting Information.

calculated resolution matrix enables the assessment of the model uncertainty (Zelt & Smith 1992). The ability for the final model to trace rays to all observed phases and a comparison of calculated and measured travel times with the picking uncertainty provides an indication of the model quality.

4.2 Modelling strategy

Although the inversion method of Zelt & Smith (1992) can invert the entire model simultaneously using all measured arrival times, the models presented here were built in a top-down approach, starting with the shallow structures constrained by seismic reflection data from the short seismic streamer and the near offset data of the OBS/H. The young and rough upper plate off southern Chile exhibits strong lateral complexity in the shallow structures, and any ambiguity in these shallow parts could cause significant distortion in the deeper structures if not eliminated early during the modelling. Some *a priori* knowledge of the existing tectonic setting and high resolution bathymetry put constraints on the starting model, and our final modelling strategy was to determine a 'minimum-parameter/prior structure' model as defined by Zelt (1999). The models were determined by automatic inversions with additional manual adjustments for model structures that are relatively complex (e.g. crossing the deformation front) or steeply dipping (rough incoming plate or forearc basement).

4.3 Final models

Each final model consists of a water layer, two sedimentary layers, an oceanic lithosphere consisting of upper- and lower-oceanic crust and mantle and subducting below the continental shelf, and a continental crustal layer landward of the Chile Margin. Aside from the reflective interfaces that determine the layer boundaries there are also two non-reflective interfaces in the model for required changes in the velocity gradient, one in the continental crust and, for Corridor 3 only, one in the oceanic lower crust. Corridors 3 and 4 also have a floating reflector (modelled using Zelt & Forsyth's (1994) algorithm) representing the decollement (from the aforementioned RV Conrad multichannel data) above the basement of the downgoing plate.

4.3.1 Corridor 4

Fig. 3 shows the TIPTEQ line that is closest to the Chile Triple Junction, sampling the youngest subducting oceanic plate which is 3 Ma at the trench. The oceanic crust is relatively thin, around 4.8 km. Sedimentary cover exists only between two basement highs

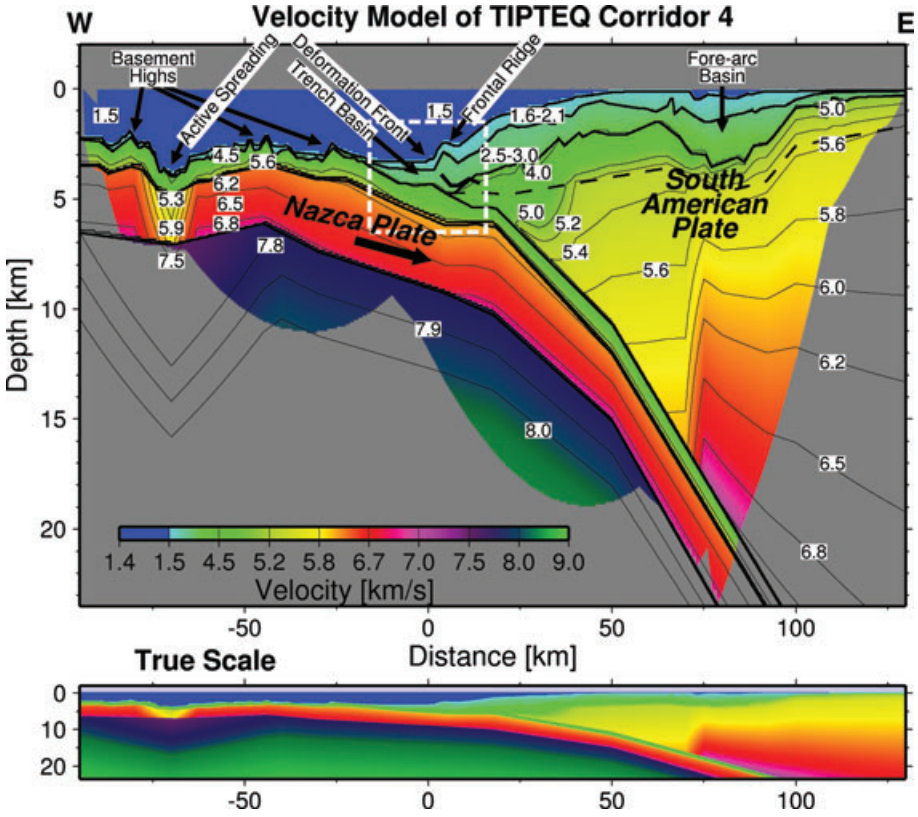

Figure 3. Proposed final velocity model of TIPTEQ Corridor 4, with velocity contours in km s^{-1}. Thicker black lines correspond to layer boundaries, dashed lines to changes in velocity gradients. Thickest black line immediately east of deformation front represents floating reflector interpreted as decollement as of multichannel seismic reflection data shown in Fig. 4. White box marks region shown in Fig. 4. Distance is given with respect to trench axis. Vertical exaggeration in top panel 6:1.

about 30 km seaward from the trench and in the trench basin which is about 15 km wide and up to 1.1 km thick. Here, the subducting plate dips about 4° and steepens to roughly 15° at the downdip data limit. Active spreading occurs about 75 km seaward off the deformation front. The resolved seismic velocities are significantly reduced around the spreading centre (Fig. 3). Away from the spreading the crustal velocities stay below 7 km s^{-1}, and mantle velocities increase from 7.5 km s^{-1} at the spreading centre to 7.8 km s^{-1} at the downdip limit of data coverage of the subducting mantle.

The deformation front is formed by a small, 10-km-wide frontal ridge that raises the seafloor by about 1 km. Landward, the continental slope gradually flattens within about 50 km off the deformation front. The sedimentary cover can be divided into three parts: (1) the downgoing sediments below the decollement, forming the subduction channel, with variable thickness between 500 and 1000 m (Fig. 4); (2) the accreted sediments in the forearc with an estimated thickness of up to 3.5 km; (3) the little deformed sediments on top of the continental crust which are on average about 2 km thick but forming a 35-km-wide and 3-km-deep forearc basin around 80 km landward from the trench (Fig. 4). East of the forearc basin the sediments are only a few hundred metres thick.

The most prominent feature of the continental shelf is the strong contrast in crustal velocities about 75 km landward off the deformation front, below the forearc basin. The topmost continental crust velocities increase landward from 4.0 km s^{-1} to about 5 km $s^{-1}$and, for example, the 5.6 km s^{-1} contour raises from about 8 km depth to 4 km depth below the forearc basin and to 2 km depth east of the basin.

4.3.2 Corridor 3

Corridor 3 (Fig. 5) is located where the age of the oceanic plate at the trench is 6.5 Ma. The oceanic lithosphere is characterised by a relatively thin, 5.2-km-thick crust with a local thickening below a seamount. Significant sediment cover (more than 100 m) commences about 125 km seaward off the deformation front, and increases strongly in thickness about 50 km seaward off the deformation front to form an up to 2-km-thick trench basin. The dip of the subducting plate is about 3° below the trench and then gradually steepening to roughly 10° towards the seismogenic zone. *P*-wave velocities in the oceanic part vary, with reduced velocities around the spreading centre (200 km seaward off the deformation front), maximum crustal velocities around 125 km seaward off the trench, and decreasing again towards the trench (Fig. 5). Oceanic mantle velocities increase from the spreading centre to a 'normal' velocity of 8.0 km s^{-1} about 75 km away from active spreading. The data do not require a reduction in mantle velocity nearer to the trench as seen in the crust above.

The slope of the continental shelf on Corridor 3 is slightly steeper than on Corridor 4, crossing a forearc high 12 km off the deformation front, and flattens within 38 km from the trench. The decollement reflector indicates a 1500–2000-m-thick subduction channel (Fig. 6). A small, 15-km wide, up to 2.5-km deep forearc basin exists around 85 km landward from the trench. West of this basin the sediments are relatively thick, on average about 1.5 km and thickening where accretion takes place; however, east of the forearc basin only a thin sedimentary cover is indicated.

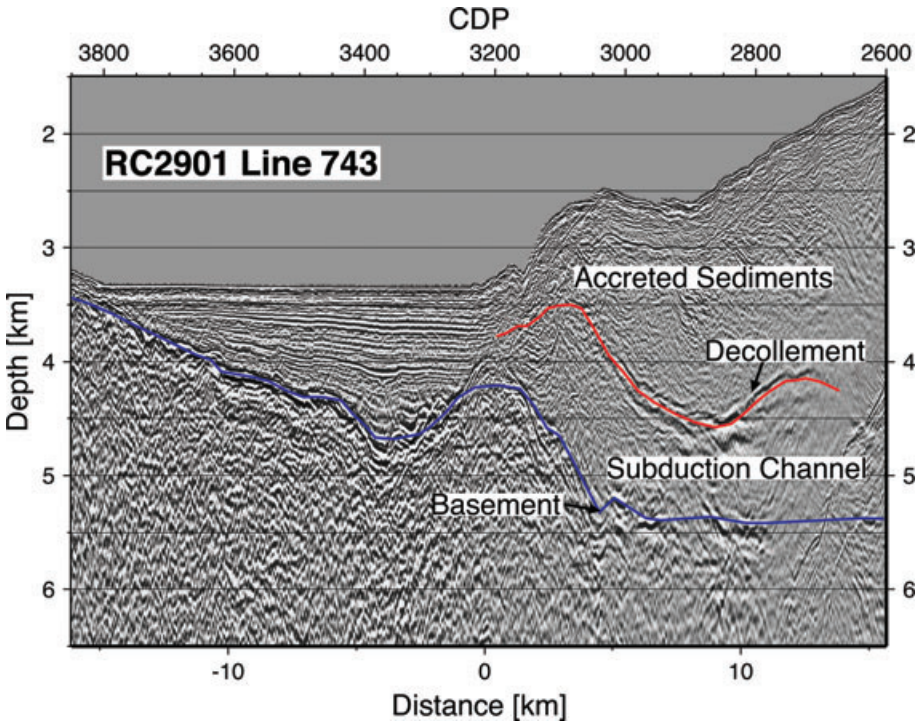

Figure 4. Multichannel seismic data from RC 2901 Line 743 from Lamont-Doherty Earth Observatory cruise in 1988 using RV CONRAD, converted to depth using the velocity model of Corridor 4. Blue line is interpreted basement reflection, red line marks interpreted decollement reflection below which sediments are subducting within the subduction channel whereas above the decollement active accretion of sediments takes place.

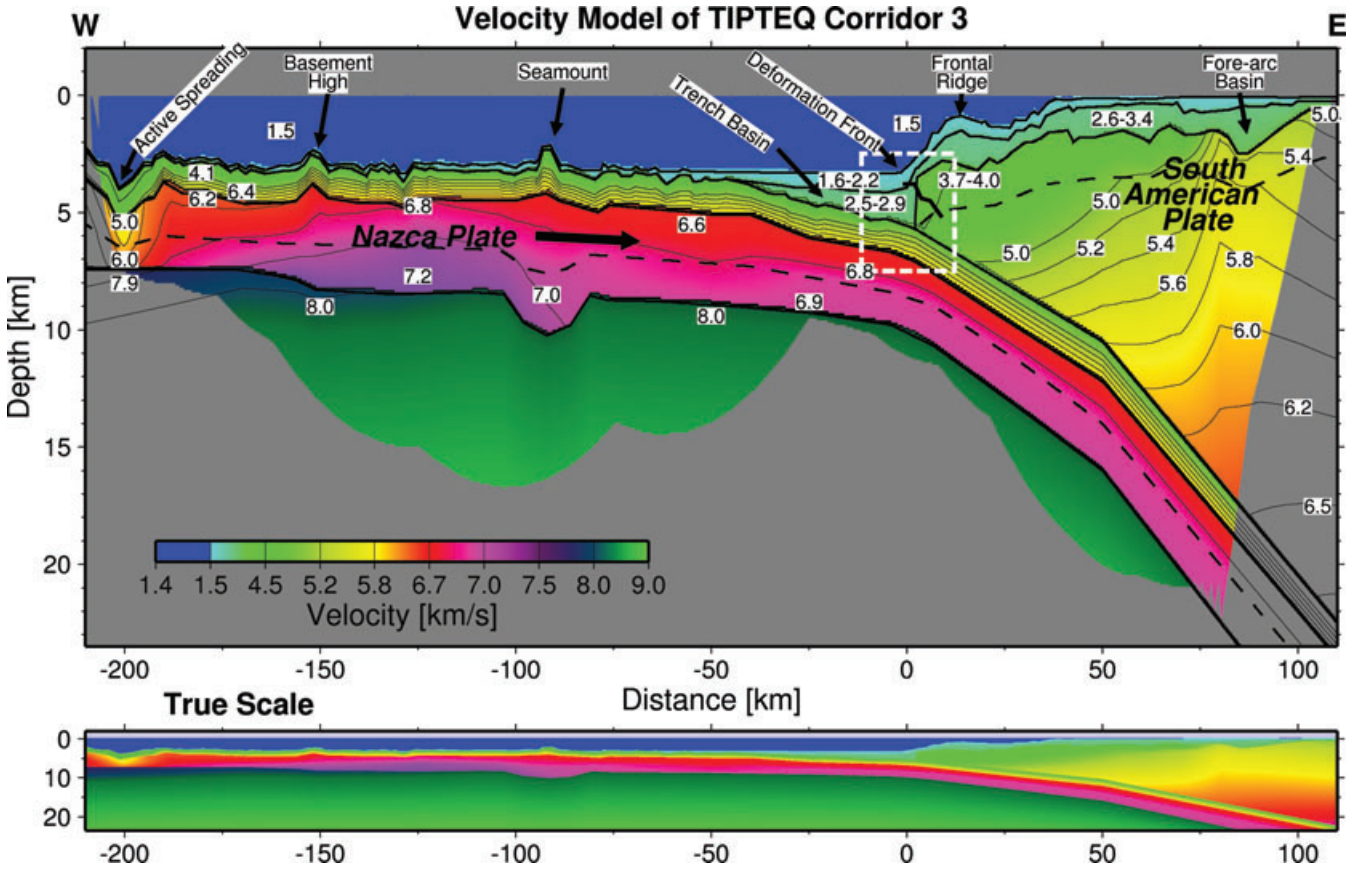

Figure 5. Proposed final velocity model of TIPTEQ Corridor 3; white box marks region shown in Fig. 6; details as of Fig. 3.

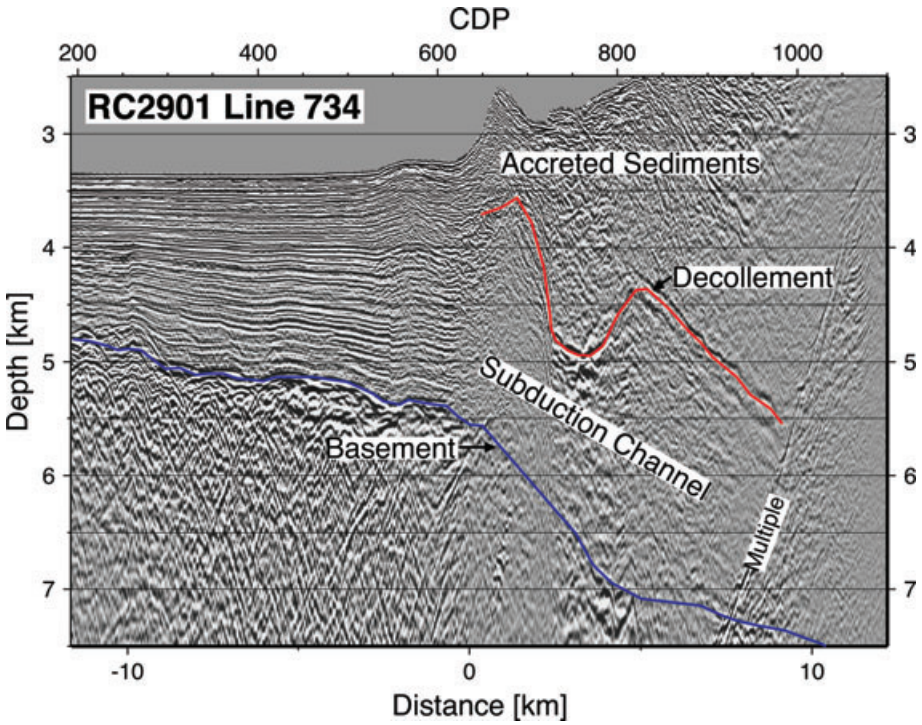

Figure 6. Multichannel seismic data from RC 2901 Line 734, converted to depth using the velocity model of Corridor 3; details as of Fig. 4.

Similar to Corridor 4, a remarkable velocity contrast exists below the continental shelf. East of 75 km off the trench the upper-crustal velocities are above 5.0 km s^{-1} with velocity gradient of about 0.1 s^{-1}. Towards the trench, the velocities are significantly reduced, indicated for example by the plunge of the 5 km s^{-1} contour in Fig. 5. As the transition between accreted sediments and slow upper continental rocks is not imaged in the seismic data, upper crustal velocities cannot be distinguished from those of accreted metasediments. Hence the velocities of the upper crust are well below 5 km s^{-1}, though without a clear lower limit.

4.3.3 Corridor 2

The complete model of this profile is shown in Fig. 7. The seaward part of the model was already described by Contreras-Reyes *et al.* (2007). An up to 5.5-km-thick crust was derived with upper oceanic lithosphere velocities decreasing significantly in the trench-outer rise area. Here we only focus on the continental shelf. The continental basement undulates below generally thickening sediments, which form a 4-km deep forearc basin on the flat part of the shelf about 75 km landward from the deformation front. East of the forearc basin the sediments are only up to 300 m thick. The dip of the downgoing plate is about 3° below the trench and up to 13° about 50 km landward from the trench.

Upper-crustal velocities are slow, less than 4 km s^{-1} near the deformation front, then increase to 4.3 km s^{-1} within 20 km. Similar to the two southern profiles, there appears a strong horizontal velocity contrast about 80 km landward from the deformation front, where the upper-crustal velocities increase rapidly to 5.2–5.4 km s^{-1}.

5 MODEL ASSESSMENT

5.1 Model resolution

Starting from the top, seafloor and sediment structures are well determined by high-resolution multibeam bathymetry and vertical seismic reflection data, respectively. The structure of the forearc basin, however, is less clear in the seismic reflection data and was primarily modelled with seismic refractions using crossover distances of crustal refractions as a measure for basement depth. Sediment velocities were determined by refractions in the trench and continental shelf.

Fig. 8 exhibits the model resolution of the subbasement structures of Corridors 2–4. The size of the symbols indicate how well the depth nodes (squares) and the velocity nodes (circles) are resolved. Calculated resolution values depend on the ray density, proximity of rays to the model nodes, and damping parameters used for the inversion. Therefore, model resolution values are to be considered as a relative measure. Resolution values vary between 1.0 (large symbol) and 0.0 (small symbol). According to Zelt & Smith (1992), nodes with resolution values greater than 0.5 can be considered as well resolved.

In general, all three models appear relatively well resolved except in the deep part around the subducting slab. Crustal velocities in the oceanic and continental part as well as upper-oceanic mantle velocities have resolution values generally above 0.75. The spreading centre at the edge of Corridor 3 (Fig. 8b) has limited data coverage in the shallow part and is therefore considerably less well resolved than the spreading centre on Corridor 4 (Fig. 8c). OBS/H stations of Corridor 2 were not deployed in the most shallow waters on the shelf yet this area was still covered with airgun shots (Fig. 2). However, as the structures appear fairly simple, only few model nodes were required here which still are reasonably well resolved.

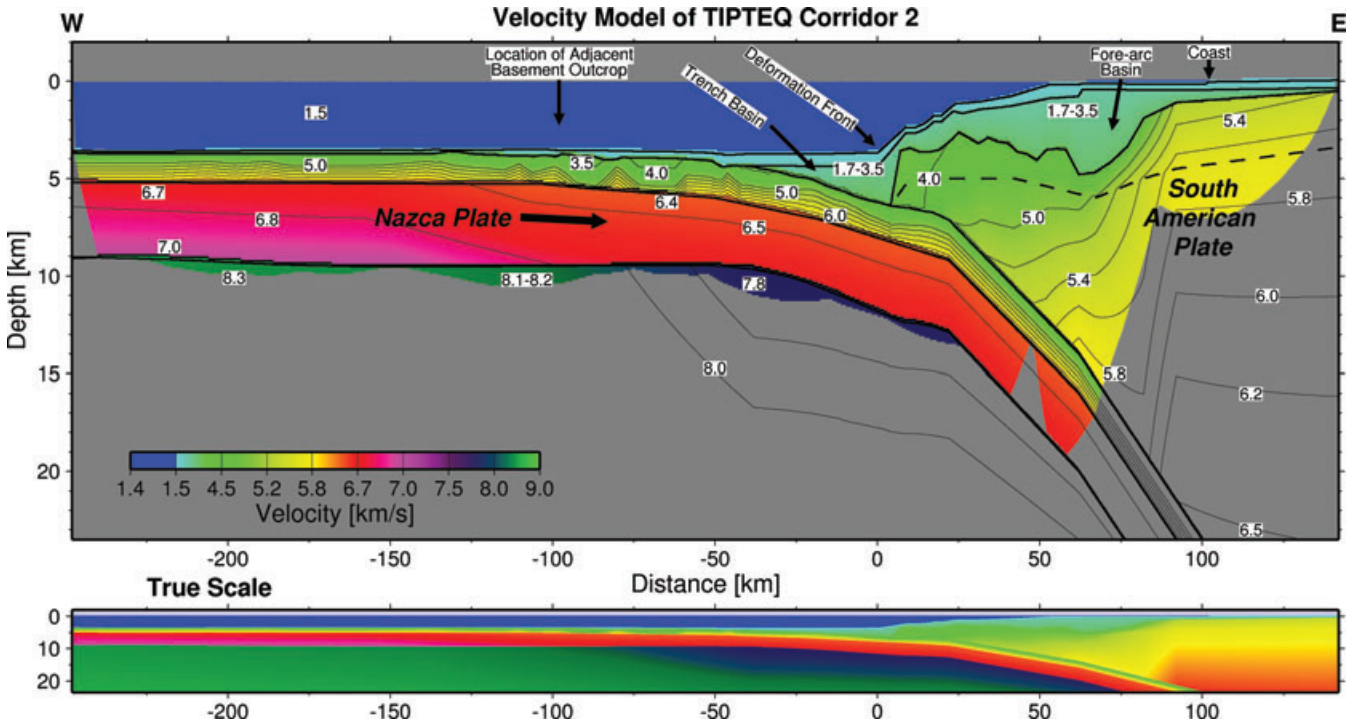

Figure 7. Proposed final velocity model of TIPTEQ Corridor 2; details as of Fig. 3. West of deformation front the model corresponds to, and is discussed by, Contreras-Reyes *et al.* (2007). Note that no data for decollement reflector were available.

Depth resolutions are reduced for the interface between upper- and lower-oceanic crust and even further reduced for the interfaces used for changing velocity gradients (dashed lines in Fig. 8). These interfaces reflect seismic signals either weakly or not at all, resulting in low-resolution values.

The data coverage of the models is shown in Fig. 9. As expected, the coverage of the lithospheric structures decreases with depth and towards the model edges. Maximum data penetration is in the region of the downgoing slab, 22 km on Corridor 3, 23 km on Corridor 4 and 19 km on Corridor 2.

5.2 Data fits and model uncertainties

The Zelt & Smith (1992) ray-tracing algorithm automatically calculates normalised chi-square values (rms misfit divided by the data uncertainty) that show how well the data fit the final model. A chi-square value greater than 1 means that the data misfit is larger than the data uncertainty, for example, a values of 4 means the misfit is twice as large as the uncertainty. Chi-square values smaller than 1 mean that the model fits the data better than required by the data uncertainty, so that for instance a simpler model may still satisfy the data. As our modelling strategy was to produce a minimum-structure model, we aimed for final models with chi-square values close to but not necessarily smaller than 1.

Picking uncertainties for all three corridors vary between 0.03 s for near offset refractions and 0.12 s for deeper reflections. In detail, the three corridors have the following normalized chi-squares: Corridor 4: 1.3 (6343 data points used with an average rms traveltime residual of 0.076 s); Corridor 3: 1.4 (8686 data points with rms misfit of 0.078 s) and Corridor 2 (shelf only): 1.4 (723 data points with rms misfit of 0.083 s).

Example data fits are shown in Figs 10(a) and (b) for Corridor 4, 11(a)–(b) for Corridor 3 and 12 for Corridor 2, respectively. Additional examples can be found in Figs S1(a)–(d), S2(a)–(f) and S3(a)–(b). The bottom panels show seismic data with predicted arrivals of all possible *P*-wave phases overlain. The central panels show actual picked and corresponding predicted arrivals. The top panels show model ray paths only to the picked arrivals, highlighting which phases actually constrain which part of the model, and only every second to fourth ray path is drawn.

Each of the data examples correspond to significant features in the models, and in order to show that the data require these features, selected phases from a slightly modified, simpler model without this feature were also calculated and drawn as dashed lines. Details are given in the figure captions. Note that this represents an optimistic estimate for the requirement of each model feature, as we exclude alternative models with different shallow structures that may allow different deeper structures to still fit the data. The assumption is that the structures determined during our top-down modelling approach are well determined in the shallow parts before the deeper structures are modelled.

Generally, Figs 10–12 and S1–S3 show a reasonable data fit usually within the data uncertainty. However, at some locations the data fit becomes marginal, such as the crustal refraction of station OBH 85 (Fig. 11b). A comparison with the actual seismic data here exhibits that the quality of the data is reduced, and the picking uncertainty may be considered as slightly underestimated. The shelf region on all corridors was found to be slightly less well fitted than the oceanic part, caused by the reverberative nature of the seismic signal (e.g. Figs 11b and S1d), and also because stations that are shallow and appear slightly off-line exhibit near-offset ambiguities that can have an effect on the reciprocity (*cf*. Fig. 11b, +18 km offset and Fig. S2f, −18 km offset). However, we consider the

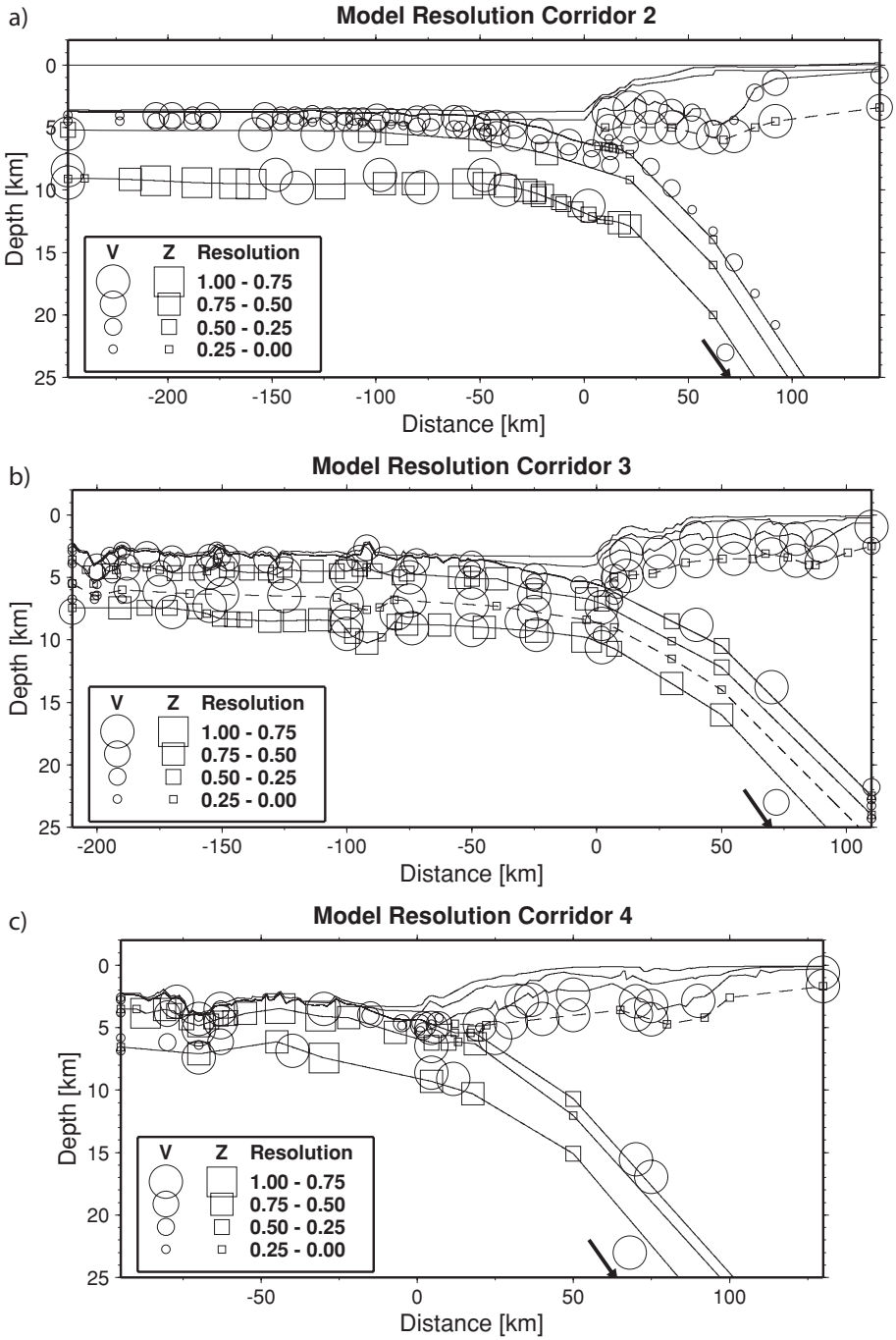

Figure 8. Model resolution for TIPTEQ Corridors 2, 3 and 4, with depth nodes (squares) and velocity nodes (circles) drawn in sizes according to their resolution. Larger symbols with values greater than 0.5 are considered well resolved. The upper-mantle velocity nodes marked with an arrow lie at the model edge outside the plotting area.

station spacing to be sufficiently close to compensate such negative effects but regard the oceanic parts to be resolved slightly more accurately.

Considering the traveltime uncertainties and misfits, the ray-geometry (penetration depth and offset), and manually changing the model parameters to examine the model space (Figs 10–12 and S1–S3), we estimate the following model uncertainties: depth to sediments: ±50–200 m; depth to crust: ±50–300 m, depth to mantle: ±100–300 m; velocity of sediments: ±100–300 m s^{-1}; velocity of crust 50–150 m s^{-1}; velocity of mantle: ±100–200 m s^{-1}. Average uncertainties are at the lower end of these values, and are generally lower for shallower nodes at high ray coverage (Fig. 9).

6 DISCUSSION

6.1 The incoming plate

One of the aims of the TIPTEQ initiative was to analyse the influence of the age of the incoming plate. Corridors 3 and 4 cover ocean crust ages from zero-age at the spreading centres of the

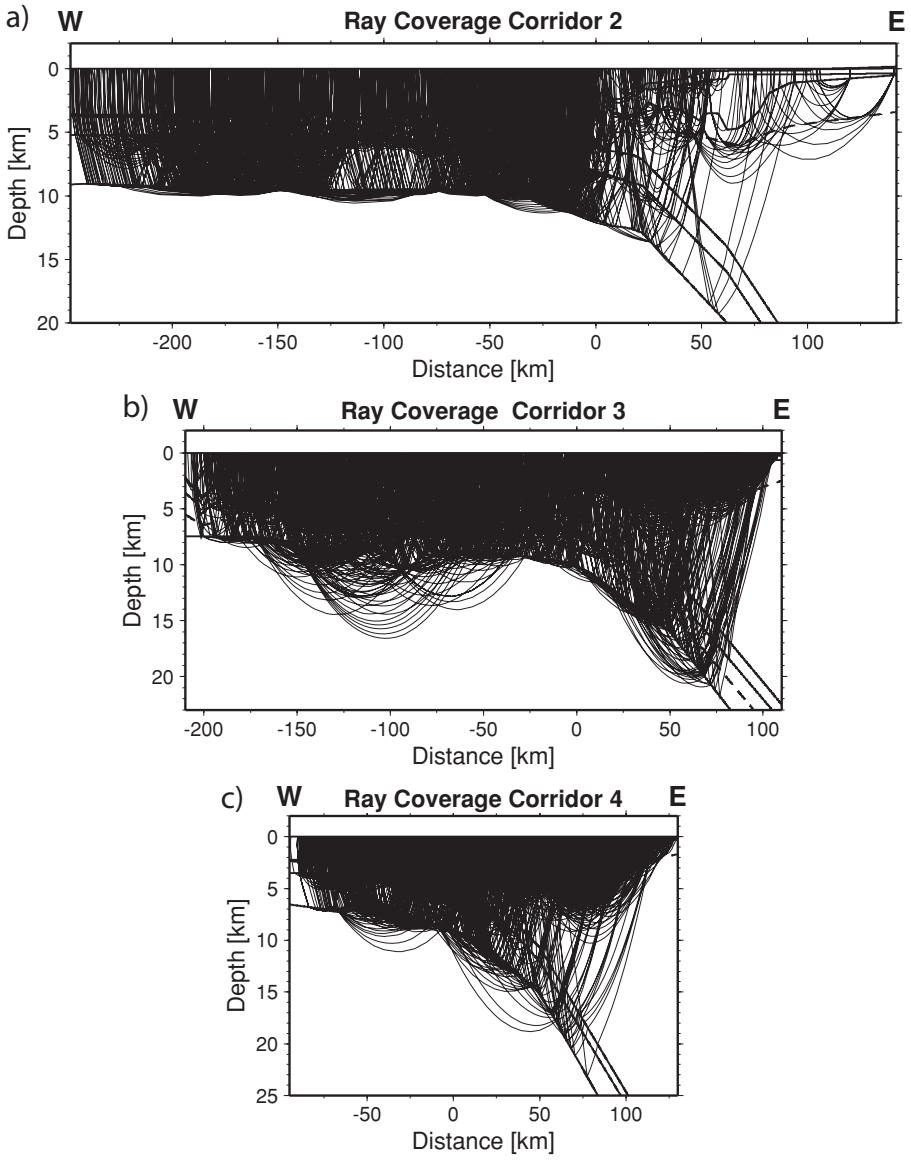

Figure 9. Data coverage for TIPTEQ Corridors 2, 3 and 4. Only every third ray is drawn for clarity. The longest line, Corridor 2, has the lowest coverage of the continental shelf structures (east of model-km 0) as OBS/H station were only deployed up to model-km 51 because of shallow water depths; shooting out to model-km 100 and also two land stations fill this gap. The deepest model penetration down to 23 km into the subduction slab is on Corridor 4 in the south, which has the farthest deployment of ocean bottom instruments landward of the trench axis, out to model-km 125. All profiles shown at same scale with vertical exaggeration 6:1.

Chile Ridge increasing towards the trench to 3.0 Ma (Corridor 4) and 6.5 Ma (Corridor 3) at the deformation front. Corridor 2 has the oldest oceanic crust of the three profiles, ranging from 8.5 Ma at the western end to 14.5 Ma at the trench. Fig. 13 compares the structures of all models analysed in this paper. In addition, for a more comprehensive discussion on the central Chilean margin, Fig. 13 also shows results from the northern TIPTEQ Corridor 1 with a plate age of 30 Ma (Contreras-Reyes *et al.* 2008b) and from the Valparaiso area at 32.8°S with a plate age of 37 Ma at the deformation front (Flueh *et al.* 1998; Zelt *et al.* 2003).

6.1.1 Seismic structures of crust and upper mantle

Each of the TIPTEQ Corridors exhibits slightly different patterns in the distribution of crustal velocity along each profile towards the trench. Whereas Corridors 1 and 2 show a distinct reduction in crustal and also upper-mantle velocities in the outer rise and trench region compared to their western, undeformed parts, Corridors 3 and 4 show only a slight velocity reduction in the crust and none in the mantle. As will be discussed below (Section 6.1.2), the velocity reduction is explained by the alteration of crust and mantle due to plate bending and possible hydration of the uppermost lithosphere. Crustal velocities are slowest in the spreading centres of Corridors 3 and 4 (averaging 3.5 km s^{-1} at the top and 4.7 km s^{-1} at the bottom of the upper crust, and 5.5 and 6.0 km s^{-1} for top and bottom of the lower crust, respectively), and they increase immediately away from active spreading. This is in accordance with plate cooling effects (e.g. Grevemeyer *et al.* 1999).

Similar to the crustal velocities, the upper-mantle velocities also show a typical increase with plate age as observed elsewhere (Grevemeyer *et al.* 1998). Corridors 1 and 2 exhibit 'normal' upper-mantle velocities, unaffected by plate bending effects, of

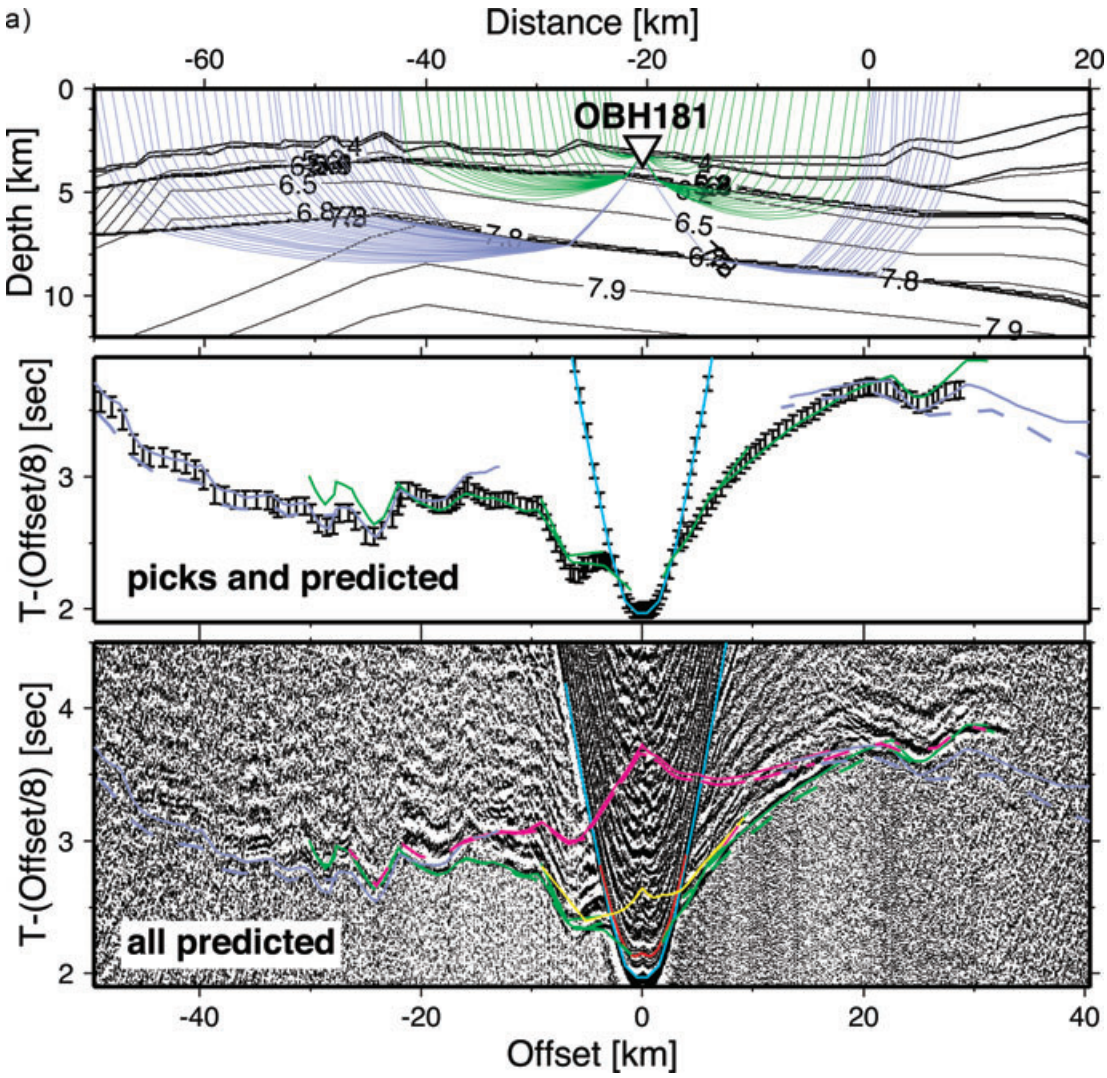

Figure 10. Examples of data fits for TIPTEQ Corridor 4. Locations are shown in Fig. 2. Bottom panels show seismic data with predicted arrivals (continuous lines) of all possible P-wave phases overlain. Central panels show actual picked and corresponding predicted arrivals plus dashed lines representing model changes as explained below. Top panels show model ray paths only to the picked arrivals, highlighting which phases actually constrain which part of the model, and only every second to fourth ray path is drawn. (a) OBH 181, highlighting both, oceanic crust at model-km −40 km (dashed: predicted arrivals with upper-mantle velocity of 8.0 km s^{-1}) and trench (dashed: predicted arrivals with Moho up to 500 m shallower); (b) OBH 171, highlighting the shelf area (dashed: predicted arrivals with upper-plate velocities of 4.5 km s^{-1} below continental slope). Other data examples are shown in Fig. S1 of the Supporting Information.

8.3–8.4 km s^{-1}. On Corridor 3 the mantle velocity is about 8.0 km s^{-1}, and Corridor 4 about 7.8 km s^{-1}. Active spreading is accompanied by reduced mantle velocities down to 7.5 km s^{-1} on Corridor 4 where the data coverage is reasonably high. Overall, the mantle velocities correlate well with those summarised by Grevemeyer *et al.* (1998). The effect of plate bending on the mantle is discussed in the following section.

Corridor 3 exhibits a region of increased velocities in the lower crust west of a small seamount (model-km −95) and east of the region of active spreading (Fig. 5). The root of the seamount is relatively localised, suggesting a seamount emplacement on a relatively young oceanic crust. As both the increase in lower crustal velocities as well as crustal thickening in the same region appear similar to what has been observed for mantle melting (e.g. Takahashi *et al.* 2008), we speculate that perhaps a small, remnant pocket of hot mantle may have caused secondary mantle melting of the lower crust in this region to explain the observed structures.

As for the crustal thickness, disregarding the vicinity of the spreading centres where oceanic crust is actively generated, average crustal thicknesses gradually increase from around 4.8 km on Corridor 4 in the south, to around 5.2 km on Corridor 3, to 5.5 km on Corridor 2, and even thicker (6–7 km) some 500 km to the north (Krawczyk *et al.* 2006; Contreras-Reyes *et al.* 2008b). The apparent trend of slightly thicker oceanic crust on progressively older corridors needs to be put into perspective with changes along the Chile Ridge. Even on the overlapping age ranges of Corridors 3 and 4 there appears a difference in crustal thickness. Therefore, this difference must stem from changes in the corresponding spreading centres at the time of crustal generation and possible 'side-effects' due to the proximity of adjacent fracture zones (White *et al.* 1992). The individual sections of the Chile Ridge spreading centre may become progressively hotter to the north, thus producing thicker crust, although the proximity of 10–20 km of Corridor 4 to the Guamblin and Darwin fracture zones (Figs 1 and 2) may be sufficiently close to

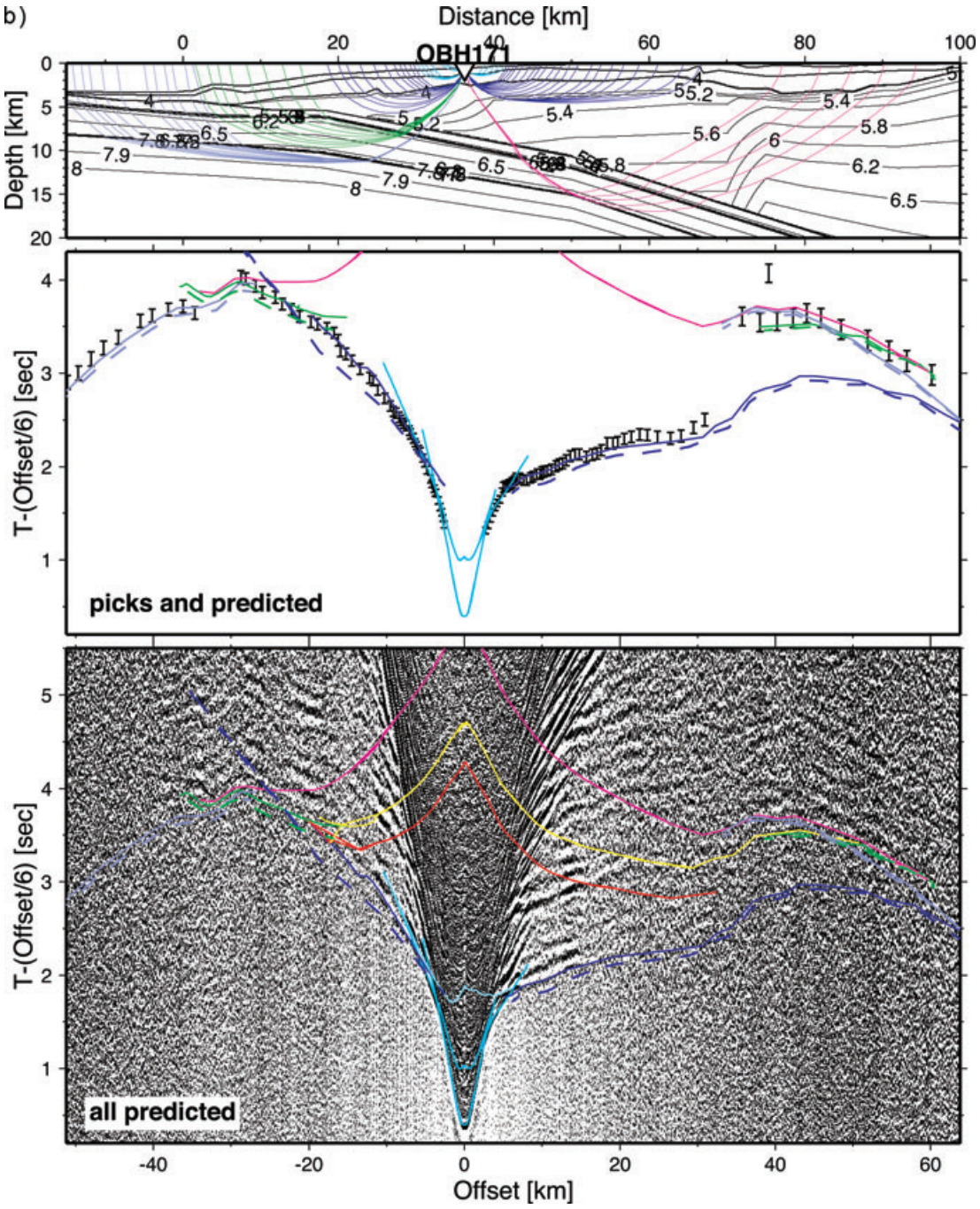

Figure 10. (*Continued.*)

have a cooling and hence thinning effect on the young plate (White *et al.* 1992).

The top of the oceanic plate is riddled with a differently sized spreading fabric and therefore appears quite rough in regions of reduced sediment cover. Smoother oceanic basement at depth and also along Corridor 2 may be attributed to artificial reflector smoothing during modelling. The roughness of the top of the subducting crust below the trench is imaged well by seismic reflection data of Corridors 4 and 3 (Figs 4 and 6) as well as on Corridor 2 (Contreras-Reyes *et al.* 2007). Furthermore, active faulting during plate bending prior to subduction (Ranero *et al.* 2003) appears to form horst and graben structures as seen on TIPTEQ Corridor 1 (Contreras-Reyes *et al.* 2008b) and may thus even increase the roughness of the upper plate.

6.1.2 Outer rise, microseismicity and hydration

The formation of the outer rise appears more pronounced in the north. This is because plate bending induces a stronger bulge on older and colder crust (Bry & White 2007). This can be seen by a comparison of bathymetry and gravity (Fig. 14), where for example Corridor 2 shows a clear positive gravity/bathymetry bulge in the outer rise area as opposed to Corridor 3. It also reflects differences

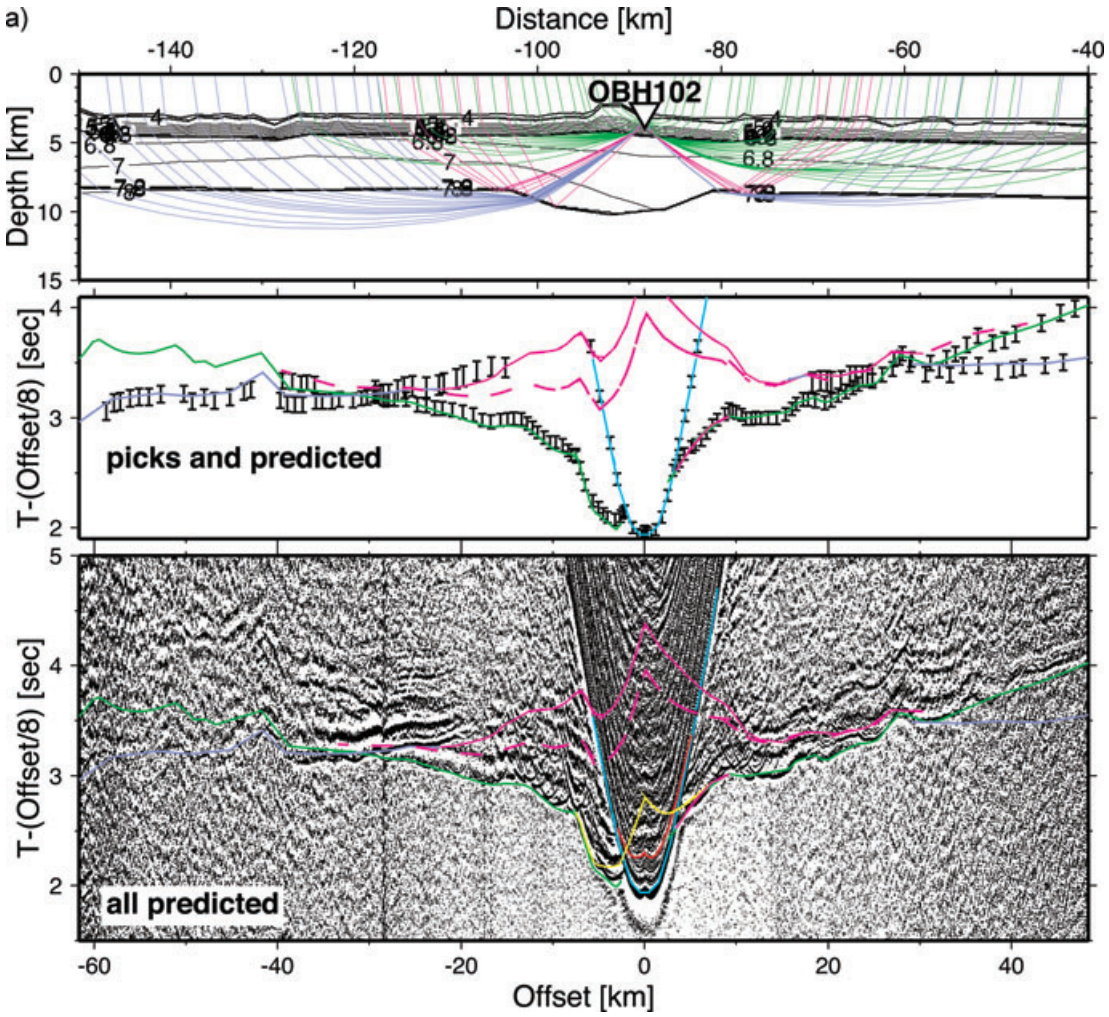

Figure 11. Examples of data fits for TIPTEQ Corridor 3. Locations are shown in Fig. 2. See Fig. 10 for a general description. (a) OBH 102, highlighting oceanic lithosphere and local crustal thickening at seamount (dashed: predicted arrivals without crustal thickening); (b) OBS 76, highlighting shelf area (dashed: predicted arrivals with strong horizontal velocity gradient shifted 20 km seaward). Other data examples are shown in Fig. S2 of the Supporting Information.

in the elastic properties and hence mechanical behaviour of the oceanic plate (Tassara *et al.* 2007).

Considering seismicity at the outer rise measured on Corridors 2 and 3 as part of the TIPTEQ project (Tilmann *et al.* 2008), the younger and also thinner plate of Corridor 3 with possibly stronger plate cooling and a less pronounced outer rise has a higher bending-related seismicity than on Corridor 2 (Tilmann *et al.* 2008). The effective elasticity of the plate of Corridor 3 seems lower (Tassara *et al.* 2007) and the small-scale fracture density may be higher and more localized than on Corridor 2.

One of the more significant results from the observed outer rise seismicity is, however, the strong indication towards water penetrating the oceanic lithosphere. Tilmann *et al.* (2008) measured a relatively high *b*-value and a significant amount of repeated earthquakes in the outer rise, and both factors seem to imply strong lithospheric hydration. This is independently corroborated by Contreras-Reyes *et al.* (2007, 2008a) and partly reproduced in this paper from seismic wide-angle data analysis. These data show strong alteration of the oceanic lithosphere at the outer rise of Corridor 2, where crustal and upper-mantle velocities are strongly reduced (Fig. 7), Poisson's ratios in the mantle are relatively high, and seismic anisotropy in the upper mantle is lowered possibly due to hydration of the upper lithosphere (Contreras-Reyes *et al.* 2008a).

A mechanism for hydrating the upper lithosphere in the outer rise is to open water pathways along bend-faulting at the outer rise (Ranero *et al.* 2003, 2005). This may work well in regions of sediment-starved incoming plate in North and Central Chile (Ranero & Sallares 2004; Ranero *et al.* 2005) or large seafloor cutting faults in Central America (Grevemeyer *et al.* 2007; Ivandic *et al.* 2008; Lefeldt & Grevemeyer 2008) where water can readily enter the crust. In southern central Chile, however, a comparably thick and homogeneous sediment blanket prevents percolation of water. On Corridor 1, which also exhibits lowered velocities in the outer rise and trench area (Fig. 13), the intersecting Mocha Fracture Zone could have allowed for water entering the upper lithosphere (Contreras-Reyes *et al.* 2008b). On Corridor 2, an adjacent piece of outcropping basement (marked in Fig. 7) could allow circulation of water, as indicated by lowered basement temperatures from heat flow measurements (Contreras-Reyes *et al.* 2007).

For Corridors 3 and 4 it is difficult to quantify a velocity reduction in the outer rise area for a lack of observed 'normal', unaltered piece of lithosphere along these profiles. Two duelling processes are active in this region: (1) plate cooling for an ageing plate with

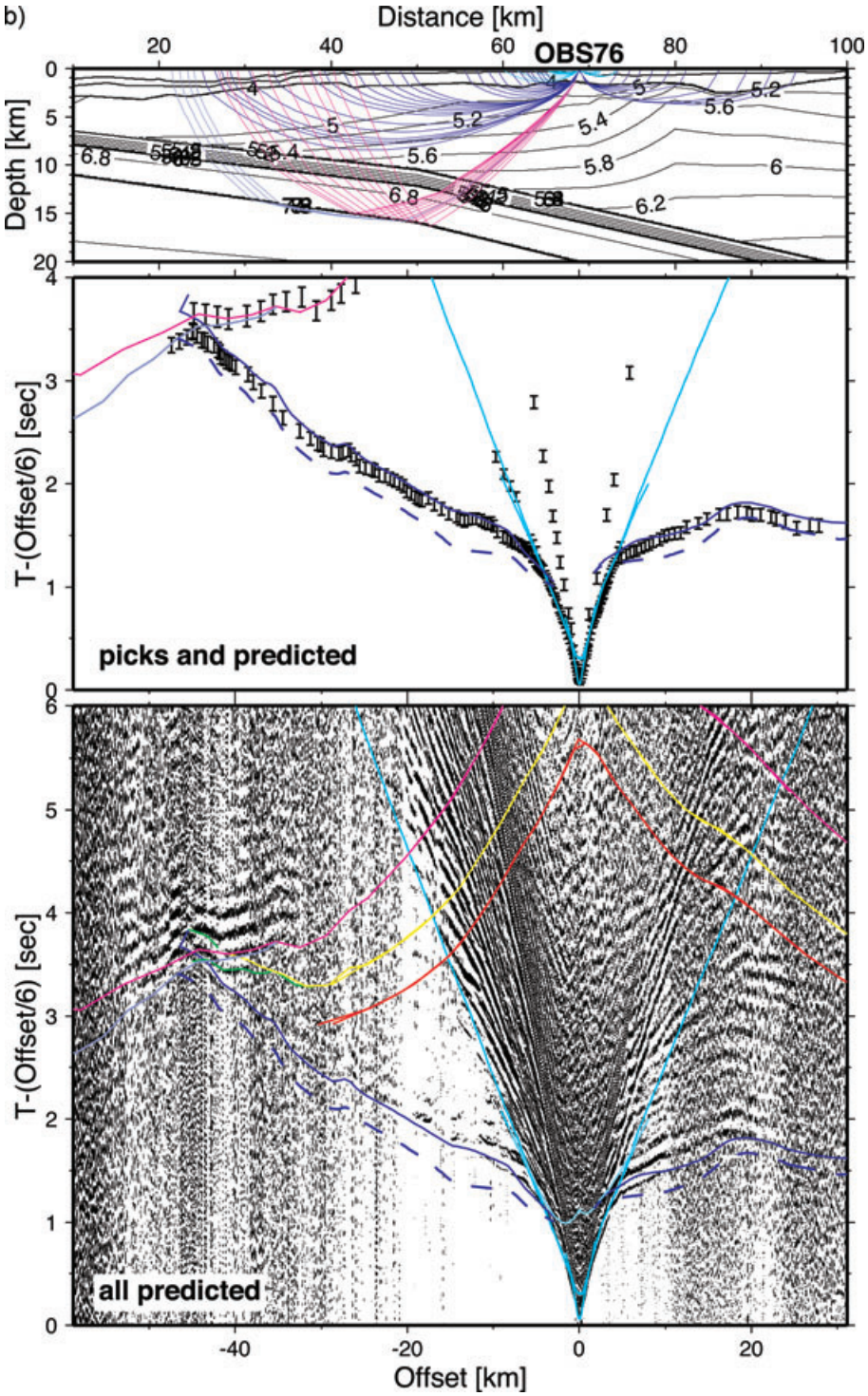

Figure 11. (*Continued.*)

associated velocity increase, versus (2) plate bending, opening of cracks and faulting with associated velocity decrease. Therefore, we are unable to argue on actual hydration of the lithosphere except that it is potentially effective given that lateral fluid flow is possible up to 50 km (Fischer *et al.* 2003) and outcropping basement and fracture zones are sufficiently close. We expect, however, that the younger and therefore hotter plate of Corridors 3 and 4 with a shallower brittle–ductile transition has a shallower depth of water infiltration into the lithosphere (Ranero & Sallares 2004), and our models appear at least consistent with this notion. In particular, the upper-mantle velocity of 8.0 km s^{-1} extending along most of Corridor 3 (Figs 5 and 13) does not indicate any necessity for serpentinization of mantle peridoties caused by fluids entering the mantle.

6.1.3 Trench basin

The trench basin along the southern central Chilean margin south of Juan Fernandez Ridge (32.5°S) is in the order of 2 km deep almost

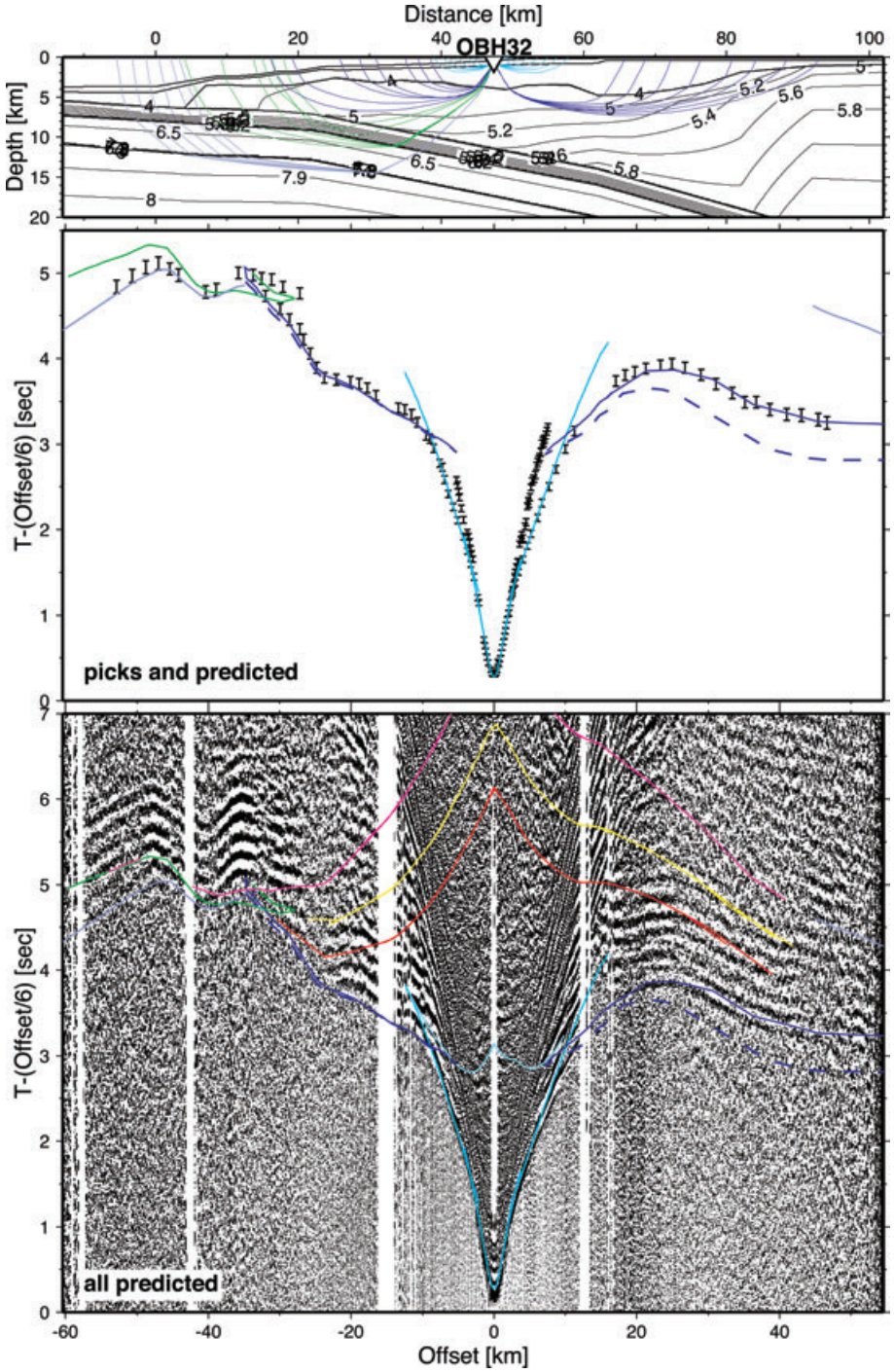

Figure 12. Examples of data fits for TIPTEQ Corridor 2. See Fig. 10 for a general description. OBH 32 (location shown in Fig. 2), highlighting shelf area (dashed: predicted arrivals with strong horizontal velocity gradient shifted 15 km seaward). Other examples for the shelf are shown in Fig. S3 of the Supporting Information. For the oceanic part, see Contreras-Reyes *et al.* (2007).

everywhere away from subduction ridges/fracture zones (Bangs & Cande 1997). The thinnest and also narrowest trench basin, on Corridor 4, is only 800 m thick which can readily be explained by its proximity to the Chile triple junction only 50 km to the south. Corridors 3 and 2 have trench basins of up to 2.2 km depth, and are typical for the rest of southern central Chile between Juan Fernandez Ridge and the Chile Triple Junction. Also their basin widths in the order of 40–50 km are normal for this region (Bangs & Cande 1997).

A few hundred metres thick sequence of pelagic to hemi-pelagic sediments spreads over the incoming plate outside the trench basin and is loaded with up to 2 km of terrigenous turbidites to form the trench basin (Bangs & Cande 1997; Voelker *et al.* 2006; Contreras-Reyes *et al.* 2008b). Onshore, a dramatic change in climate conditions occurs between 33°S and 46°S. More than twice as much rainfall is responsible for a significantly larger sediment supply in the south compared to the north (Bangs & Cande 1997). However, together with a northward increased water depth and the existence

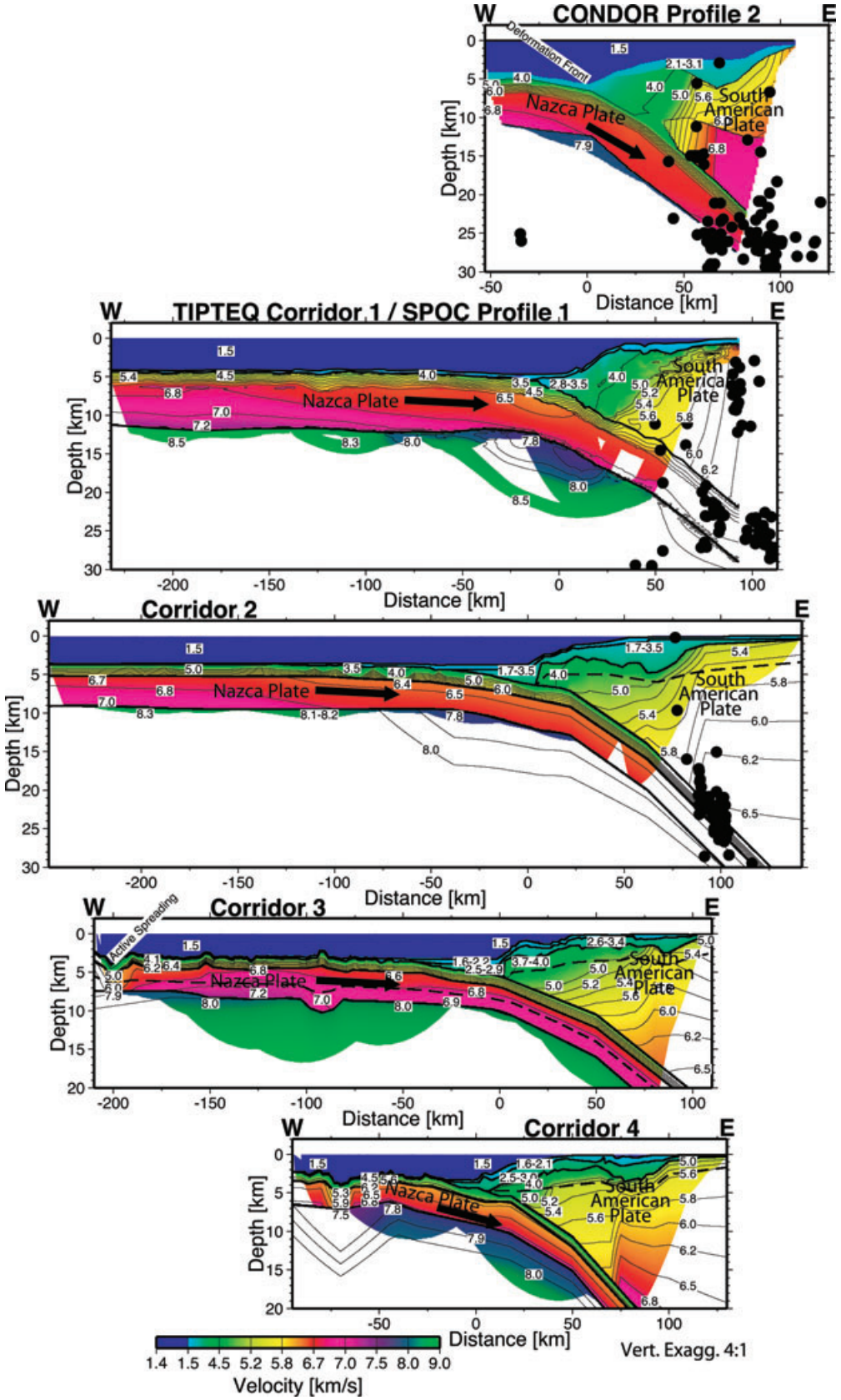

Figure 13. Comparison of all final models drawn at same scale and offset to nearly match trench axis. Also shown are results from TIPTEQ Corridor 1 (Contreras-Reyes *et al.* 2008b) and CONDOR Profile 2 (Flueh *et al.* 1998; Zelt *et al.* 2003) for structural comparison along the entire accretionary part of the central Chile margin. Locations of lines are shown in Fig. 15. The northern three models show earthquake hypocentres recorded on temporary onshore-offshore seismic networks (Thierer *et al.* 2005; Haberland *et al.* 2006; Lange *et al.* 2007), projected onto the profiles from up to 50 km from either side, indicating coincidence of strong lateral velocity gradient within continental crust and intraslab seismicity.

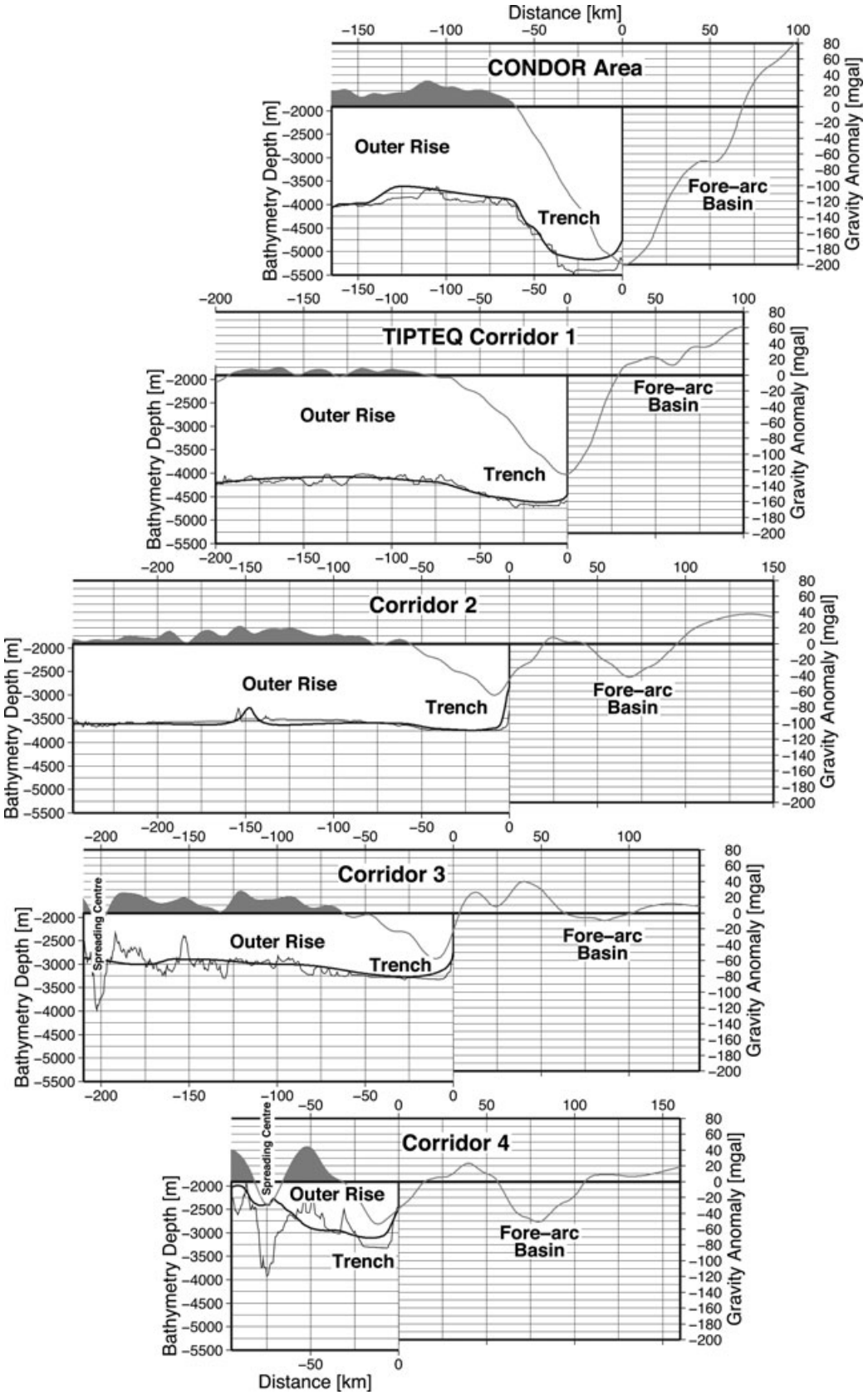

Figure 14. Bathymetry and Bouguer satellite gravity along TIPTEQ lines and CONDOR area (just south of CONDOR Profile 2 (Fig. 15) avoiding the seamount). Positive gravity anomalies (right ordinate axis) in the outer rise area are shaded in grey, with the grey line continuing landward. Bathymetry (left ordinate axis) are both GEBCO (smooth thick black line) as well as high-resolution multibeam sonar (thin black line) data. Areas of outer rise, trench, forearc basin and spreading centre are marked. Corridor 2 and north of it clearly exhibit a bulging outer rise whereas the southern corridors produce a more general trenchward decrease of gravity and bathymetry overprinted with high frequency anomalies.

of a 1000-km-long axial channel along the Chile trench north of 41°S (Fig. 15) (Voelker *et al.* 2006), the trench basin geometries demonstrate a highly efficient sediment transport to the north where the Juan Fernandez Ridge forms a barrier against the sediment flow. The sediments are distributed rather evenly in the trench region, as indicated by a smooth seafloor of 40–50 km width (Fig. 15), ensuring a homogeneous trench.

6.2 The subduction channel

The sediment above the decollement (Figs 4 and 6) is included in the accretionary prism of the upper plate (discussed below in Section 6.3.1) whereas the lower part forms the subduction channel of downgoing sediment. The location of the decollement reflector on Corridors 3 and 4 indicates that on average about 500 m of the incoming sediment is accreting which, considering the different trench basin thicknesses, translates into roughly three quarters of subducting incoming sediments on Corridor 3 and one third of subducting incoming sediments on Corridor 4.

A relatively thick subduction channel has also been observed on other seismic reflection lines south of the Mocha Fracture Zone (Bangs & Cande 1997; Diaz-Naveas 1999). Corridor 3 may therefore show a typical subduction channel for the area between the Chile Triple Junction and the Mocha Fracture Zone, with three quarters of the trench fill bypassing.

A thinner subduction channel is only observed at the location of Corridor 4 and also 30 km south, immediately north of the Chile Triple Junction (line 745, along sites of Ocean Drilling Program Leg 141; Behrmann *et al.* 1994). However, the latter two lines may be atypical for southern central Chile as they are in the vicinity of the incoming Chile Ridge, with a thin or currently absent trench basin at the deformation front, and most or all sediments here are currently accreted frontally at the toe of the frontal slope (Behrmann & Kopf 2001). Here in the south, the Chile Ridge itself is about to erode the upper plate (Bourgois *et al.* 2000). North of the Mocha Fracture Zone, the subduction channel is also thinner than south of it (Bangs & Cande 1997; von Huene *et al.* 1997; Diaz-Naveas 1999).

For the region of the thick subduction channel it has been argued that the seismic reflection data indicate basal accretion of the top of the channel (Bangs & Cande 1997; Diaz-Naveas 1999) by means of compaction and dewatering of the upper part of the subduction channel which attaches to the upper plate (Diaz-Naveas 1999). Considering the seismic velocities in the forearc (Fig. 13), underplating may only occur within 50 km from the deformation front, though reduced resolution for deeper velocities and the inability of the refraction method to detect small low velocity layers at depth could prevent us from identifying underplating.

The possible role of the subduction channel in megathrust earthquakes is discussed below in Section 6.4.

6.3 The continental plate

On all three newly analysed corridors, the overriding continental South American Plate exhibits two zones of distinct forearc structures (1) a frontal slope with highly reduced shallow velocities before the onset of the active backstop and (2) a continental shelf with a remarkably strong lateral velocity gradient in the vicinity of a forearc basin (Figs 3, 5 and 7). It is also apparent that some structural differences between the corridors exist although, even taking

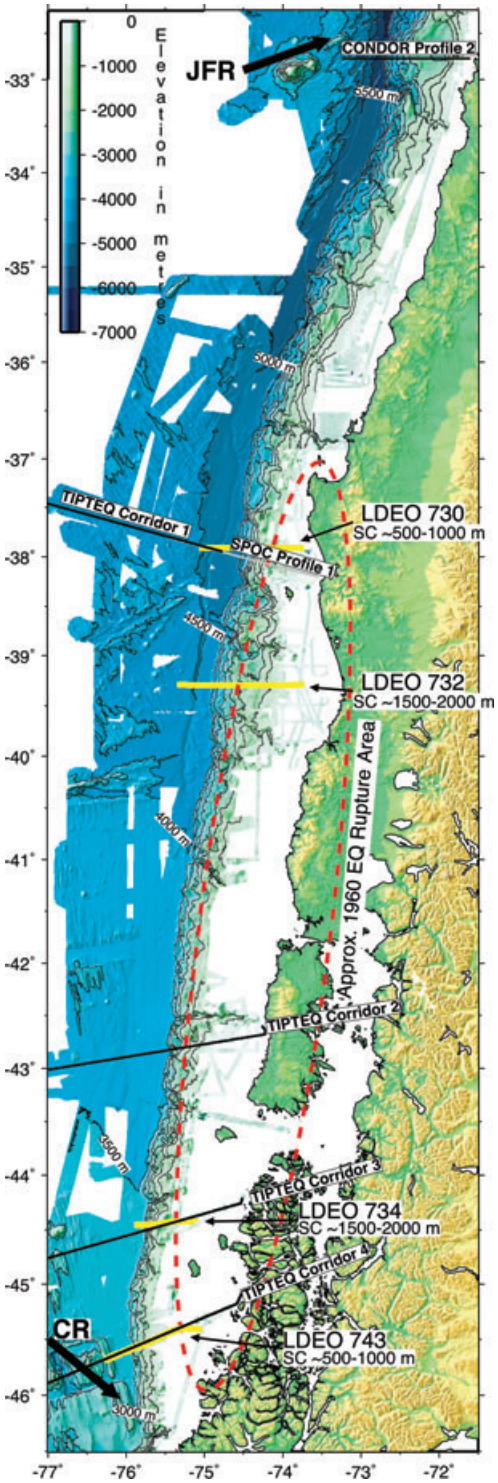

Figure 15. Map of entire accretionary part of the central Chilean margin between the Juan Fernandez Ridge (JFR) in the north and the Chile Ridge (CR) in the south, demonstrating northward increasing water depth from 3000 to 5500 m, smooth seafloor of the 40–50 km wide trench basin, and an axial channel north of 41°S. In addition, the rupture area of the 1960 great Chile earthquake (Barrientos & Ward 1990) and the thickness of the subduction channel is marked to emphasise the spatial correlation of subduction channel thickness and terminus of the rupture. Offshore high-resolution bathymetry from RV Sonne cruises SO101, SO161, SO181, RV Meteor cruise M67/1 (Weinrebe & Schenk 2006) and from RV L'Atalante cruise CTJ (Bourgois *et al.* 2000). Land topography from SRTM (Farr *et al.* 2007).

into account results from data further north (Fig. 13), no systematic change can be observed.

6.3.1 Continental slope

The continental slope is between 35 and 50 km wide, interspersed seaward either with a few undulations within the last 25 km before the deformation front on Corridor 2, or a more pronounced frontal ridge in the same area on Corridor 3, or a small frontal ridge immediately landward from the deformation front on Corridor 4. Below the frontal parts of the continental slope velocities below 4.0 km s^{-1} increase to over 4.5 km s^{-1} around 30–40 km landward from the deformation front. This 30–40 km wide region of low velocities can be interpreted as the active accretionary prism, similar to what is observed a few hundred km further north near Arauco peninsula at TIPTEQ Corridor 1 and the SPOC profiles (Figs 13 and 15; Krawczyk *et al.* 2006; Contreras-Reyes *et al.* 2008b) and also as interpreted on seismic reflection data (Bangs & Cande 1997; von Huene *et al.* 1997). This prism would have been accumulated within the last 1–2 Myr while active accretion has been continuous after episodes of subduction erosion and accretion (Bangs & Cande 1997; Behrmann & Kopf 2001).

6.3.2 Forearc basin

The continental shelf in the area of Corridors 2–4 is underlain by the Chiloe forearc basin (Gonzalez 1989; Melnick & Echtler 2006). It extends from 41.5°S down to the Chile Triple Junction. The Chiloe Basin consists mainly of Mesozoic to possibly Late Cretaceous marine clastics, overlain by up to 1000 m of Tertiary and up to 500 m of Pliocene to Quaternary clastics (Gonzalez 1989). Structures within the forearc basin sequences allow a reconciliaton of forearc deformation, in particular basin growth and extensional normal faulting during subduction erosion before 3 Ma and uplift and basin inversion during accretion after 3 Ma ago (Melnick & Echtler 2006). Plate coupling at the subduction interface also affects forearc subsidence as indicated by gravity anomalies (Hackney *et al.* 2006), and deeper forearc basins may indicate stronger subsidence due to stronger plate coupling, which is discussed further in Section 6.4.

Corridors 2–4 cross the basin at parts that are relatively different in size and shape. Corridor 2 shows the largest part of the basin, gradually deepening from half-way up the slope over a distance of 50 km to a maximum depth of 4 km about 65 km from the deformation front (Figs 7 and 13). On Corridor 3, the smallest part of the Chiloe basin is sampled, at about 85 km from the deformation front, to a maximum depth of 2.5 km and a width of about 10 km (Figs 5 and 13). Finally, Corridor 4 shows a 25-km wide section of the forearc basin centred around 80 km from the deformation front; its maximum depth being 3 km (Figs 3 and 13). The gravity signal shown in Fig. 14 agrees with the basin structures.

6.3.3 Forearc transition zone

Regardless of the diversity in shape of the shallow forearc, the most remarkable feature on all corridors is the strong lateral velocity gradient in the continental crust some 75–80 km landward off the deformation front, directly beneath the forearc basin. All corridors have in common a marked seaward decrease in upper continental basement velocities from over 5.0–5.4 km s^{-1} down to around 4.5 km s^{-1} within about 10 km. We consider the eastern, fast velocities as normal, typical for the crystalline basement of the coastal cordillera (Mordohovich 1974). West of the velocity transition, between the coastal cordillera and the active accretionary prism we may observe a 25–50 km wide palaeo-accretionary complex as suggested by Melnick *et al.* (2006).

This strong velocity transition zone below the forearc was also detected off Arauco peninsula (Contreras-Reyes *et al.* 2008b) and Valparaiso (Flueh *et al.* 1998; Zelt *et al.* 2003), as can be seen on Fig. 13. For TIPTEQ Corridor 1/SPOC Profile 1 it has already been argued to show palaeo-accretionary structures (Contreras-Reyes *et al.* 2008b), and, considering the reduced data coverage and possibly different modelling schemes, the similarity of the inferred structures compared to the southern lines is remarkably high (Fig. 13). Off Valparaiso in the north (Fig. 15), CONDOR Profile 2 (Fig. 13) represents the northernmost part of the accretionary central Chilean margin. Magnetic anomalies here may indicate that this forearc transition zone coincides with a pre-Jurassic magmatic arc (Yanez *et al.* 2001) and may therefore be different to the south.

A significant correlation exists between the forearc transition zone and intraplate seismicity as observed on Corridors 1 and 2 and also on CONDOR Profile 2 (Fig. 13) (Thierer *et al.* 2005; Haberland *et al.* 2006; Lange *et al.* 2007). The forearc deformation occurs aseismic up to the transition zone, and similarly the interplate seismicity at the plate coupling zone is more concentrated below the transition zone and greatly reduced or absent trenchward to the west.

Overall, the forearc structures along almost 1500 km of the accretionary plate margin between the Chile Triple Junction and the Juan Fernandez Ridge are remarkably similar, including (1) the width of the 35–50 km wide accretionary prisms (2) the 25–50 km wide zone of intermediate seismic velocities representing a palaeo-accretionary complex at least in the south, and moreover (3) the sharp transition below the forearc basin with almost subvertical isovelocity contours coinciding with the onset of intraplate seismicity at the edge of the coastal cordillera (Fig. 13).

6.4 Structural implication on the seismogenesis

Our data illuminate the structures involved in the largest ever instrumentally recorded earthquake, the $M_w = 9.5$ event of 1960 (Cifuentes 1989; Barrientos & Ward 1990). TIPTEQ Corridor 1 is in-line with the epicentre of this event which was located about 50 km inland, 100 km from the trench axis (Krawczyk *et al.* 2006). This megathrust event then propagated up the seismogenic zone and all the way south to just south of our Corridor 4 (Fig. 15) (Barrientos & Ward 1990).

Although our models place constraints on thermal models determining the seismogenic zone (Voelker *et al.* 2007), our detailed structures do not reveal any features impacting directly on rupture propagation such as high relief on, or a strongly varying dip of, the downgoing plate. Therefore, it appears that the structural similarities of the south central Chilean subduction zone may have allowed the enormous rupture length of the 1960 event, as it propagated right through segments of little structural variation despite the strong thermal variation.

One factor that differs throughout the rupture area of the 1960 event is the forearc basin geometry, a possible indicator of forearc subsidence as a response to plate coupling (Song & Simons 2003; Hackney *et al.* 2006). If correct, the megathrust earthquake started in a relatively weakly coupled area (Corridor 1, small forearc basin),

propagated southward and triggered rupture in an area of stronger coupling (Corridor 2, large basin), continued across weaker coupling (Corridor 3, small basin), and finally stopped just south of an area of stronger coupling (Corridor 4, large basin). Our structural models do not indicate any evidence for the reason behind different plate coupling in the area, and so we conclude that varying patterns in rigidity and frictional coupling are rather a response to segmentation of the Chilean margin in terms of sediment consolidation, forearc rheology or possible other compositional differences (Hackney *et al.* 2006).

The remaining question is what terminated rupture propagation after cutting across six major fracture zones. From a structural point of view, the major difference between the rupture area and the areas north and south of it is the apparent thickness of the subduction channel as discussed above. The thick subduction channel along the rupture zone may have provided enough smoothness for a long rupture propagation across the fracture zones involved (Scholl *et al.* 2007). The thin subduction channels north of the Mocha and south of the Darwin Fracture Zones were too thin to reduce plate coupling, and rupturing ceased before crossing the Mocha Fracture Zone and the Chile Ridge in the north and south, respectively (Fig. 15), as opposed to what occurred 2007 off the Solomon Islands where the rupture went across the Simbo Ridge (Taylor *et al.* 2008).

7 CONCLUSION

Seismic wide-angle data from three profiles offshore southern central Chile reveal structures of the differently aged subducting Nazca and the overriding South American Plate. Well-constrained structural models show relatively thin oceanic plate thickening from 4.8 km near the Chile triple junction to 5.5 km on 14 Myr older crust in the north. This trend does not reflect dependence on plate age but more likely temperature of the spreading centre at the Chile Ridge.

Some differences exist in the formation of the outer rise which appears more developed on older crust to the north but is accompanied by less bending related outer rise seismicity compared to the younger and hotter southern oceanic lithosphere. In the region of the outer rise, a strong reduction of seismic wave velocities indicate strong alteration of the plate due to the formation of fractures and possible hydration of the oceanic lithosphere. This effect is more pronounced on the older structures in the north but may be overprinted by plate cooling effects in the south.

Towards the deformation front, the trench basin is typically about 2 km deep except in the vicinity of the buoyant and eroding Chile Ridge subducting at the triple junction in the south where it is smaller. An efficient sediment transport to increasing water depth northward is indicated. About three quarters of the trench sediments enter below the decollement and the rest are accreted except, again, in the south where the smaller trench basin provides one third of is sediment to the subduction channel, which has varying thickness, though.

The structure of continental South American Plate exhibits some variation in the shallow structure (such as the shape of continental slope and geometry of forearc basin) but strong similarities exist in the width of the active accretionary prism (35–50 km) and the occurrence of a boundary between a palaeo-accretionary complex and the coastal cordillera at around 75–80 km landward off the deformation front. The latter boundary coincides with high intraplate seismicity. A comparison with other structural models shows that the entire 1500 km of currently accretionary central Chilean margin appear remarkably similar.

Considering the similarity of the continental crustal structure, there appears little influence from the incoming plate, which itself is also relatively similar in structure though with a different thermal state and thus does not appear as a controlling factor for the propagation of megathrust earthquakes. Only the thickness of the subduction channel correlates with the rupture area of the 1960 Chile event, which ruptured through an area of a thick subduction channel that reduced plate coupling, and ceased in the area of a thinning subduction channel.

ACKNOWLEDGMENTS

We gratefully acknowledge the splendid cooperation of captains Kull and Mallon and the officers and crew of RV *Sonne* cruise 181 for a highly successful data acquisition, and thank the Editor, Thorsten Becker, and Colin Zelt and an anonymous reviewer for their highly constructive criticism, which greatly improved this paper. This paper represents publication GEOTECH-1231 of the Research and Development Programme GEOTECHNOLOGIEN funded by the German Ministry of Education and Research (BMBF) and the German Research Foundation (DFG), grants 03G0594E and 03G0181A. All figures were generated with GMT (Wessel & Smith 1998).

REFERENCES

Angermann, D., Klotz, J. & Reigber, C., 1999. Space-geodetic estimation of the Nazca-South America Euler vector, *Earth planet. Sci. Lett.,* **171**(3), 329–334.

Bangs, N.L. & Cande, S.C., 1997. Episodic development of a convergent margin inferred from structures and processes along the Southern Chile margin, *Tectonics,* **16,** 489–503.

Barrientos, S.E. & Ward, S.N., 1990. The 1960 Chile earthquake: inversion for slip distribution from surface deformation, *Geophys. J. Int.,* **103,** 589–598.

Behrmann, J.H. & Kopf, A., 2001. Balance of tectonicall accreted and subducted sediment at the Chile Triple Junction, *Int. J. Earth Sci.,* **90,** 753–768.

Behrmann, J.H., Lewis, S.D., Cande, S.C. & ODP Leg 141 Scientific Party, 1994. Tectonics and geology of spreading ridge subduction at the Chile Trple Junction: a synthesis of results from Leg 141 of the Ocean Drilling Program, *Geol. Rundsch.,* **83,** 832–852.

Bialas, J. & Flueh, E.R., 1999. Ocean bottom seismometers, *Sea Technol.,* **40**(4), 41–46.

Bourgois, J., Guivel, C., Lagabrielle, Y., Calmus, T., Boulegue, J. & Daux, V., 2000. Glacial-interglacial trench supply variation, spreading-ridge subduction, and feedback controls on the Andean margin development at the Chile triple junction area (45–48°S), *J. geophys. Res.,* **105**(B4), 8355–8386.

Brasse, H., Kapinos, G., Li, Y., Mütschard, L., Soyer, W. & Eydam, D., 2009. Structural electrical anisotropy in the crust at the South-Central Chilean continental margin as inferred from geomagnetic transfer functions, *Phys. Earth planet. Inter.,* **173**(1–2), 7–16.

Bry, M. & White, N., 2007. Reappraising elastic thickness variation at oceanic trenches, *J. geophys. Res.,* **112,** B08414, doi:10.1029/2005JB004190.

Cande, S.C. & Leslie, R.B., 1986. Late Cenozoic tectonics of the Chile trench, *J. geophys. Res.,* **91,** 471–496.

Cifuentes, I.L., 1989. The 1960 Chilean Earthquake, *J. geophys. Res.,* **94**(B1), 665–680.

Cisternas, M. *et al*., 2005. Predecessors of the giant 1960 Chile earthquake, *Nature,* **437,** 404–407.

Contreras-Reyes, E., Grevemeyer, I., Flueh, E.R., Scherwath, M. & Heesemann, M., 2007. Alteration of oceanic subducting lithosphere at the southern central Chile trench-outer rise, *Geochem. Geophys. Geosyst.,* **8,** Q07003, doi:10.1029/2007GC001632.

Contreras-Reyes, E., Grevemeyer, I., Flueh, E.R., Scherwath, M. & Bialas, J., 2008a. Effect of trench-outer rise bending-related faulting on seismic Poisson's ratio and mantle anisotropy: a case study offshore of Southern Central Chile, *Geophys. J. Int.,* **173**(1), 142–156, doi:10.1111/j.1365-246X.2008.03716.x.

Contreras-Reyes, E., Grevemeyer, I., Flueh, E.R. & Reichert, C., 2008b. Upper lithospheric structure of the subduction zone offshore of southern Arauco Peninsula, Chile at ∼38° S, *J. geophys. Res.,* **113,** B07303, doi:10.1029/2007JB005569.

Currie, C.A., Hyndman, R.D., Wang, K. & Kostoglodov, V., 2002. Thermal models of the Mexico subduction zone: implications for the megathrust seismogenic zone, *J. geophys. Res.,* **107**(B12), 2370, doi:10.1029/2001JB000886.

DeMets, C.G., Gordon, R.G., Argus, D.F. & Stein, S., 1994. Effect of recent revisions to the geomagnetic time scale on estimates of current plate motions, *Geophys. Res. Lett.,* **21,** 211–214.

Diaz-Naveas, J.L., 1999. Sediment subduction and accretion at the Chilean convergent margin between 35° und 40°S, *PhD thesis*. Ch.-A.-Univ., Kiel, Germany.

Farr, T.G. *et al*., 2007. The Shuttle Radar Topography Mission, *Rev. Geophys.,* **45,** RG2004, doi:10.1029/2005RG000183.

Fischer, A.T. *et al*., 2003. Hydrothermal recharge and discharge across 50 km guided by seamounts on a young ridge flank, *Nature,* **421,** 618–621.

Flueh, E.R. & Bialas, J., 1996. A digital, high data capacity ocean bottom recorder for seismic investigations, *Int. Underwater Syst. Design,* **18**(3), 18–20.

Flueh, E.R. *et al*., 1998. Seismic investigation of the continental margin off- and onshore Valparaiso, Chile, *Tectonophys.,* **288,** 251–263.

Gonzalez, E., 1989. Hydrocarbon resources in the coastal zone of Chile, in *Geology of the Andes and its Relation to Hydrocarbon and Mineral Resources,* Vol. 11, pp. 383–404, eds Ericksen, G., Canas Pinochet, M.T. & Reinemund, J.A., Houston, Texas, Circum-Pacific Council for Energy and Mineral Resources Earth Science Series.

Grevemeyer, I., Weigel, W. & Jennrich, C., 1998. Structure and ageing of oceanic crust at 14°S on the East Pacific Rise, *Geophys. J. Int.,* **135,** 573–584.

Grevemeyer, I., Kaul, N., Villinger, H. & Weigel W., 1999. Hydrothermal activity and the evolution of the seismic properties of upper oceanic crust, *J. geophys. Res.,* **104**(B3), 5069–5080.

Grevemeyer, I., Ranero, C.R., Flueh, E.R., Klaeschen, D. & Bialas, J., 2007. Passive and active seismological study of bending-related faulting and mantle serpentinization at the Middle America trench, *Earth planet. Sci. Lett.,* **258,** 528–542, doi:10.1016/j.epsl.2007.04.013.

Gross, K., Micksch, U. & TIPTEQ Research Group, Seismics Team, 2008. The reflection seismic survey of project TIPTEQ-the inventory of the Chilean subduction zone at 38.2 degrees S, *Geophys. J. Int.,* **172**(2), 565–571.

Haberland, C., Rietbrock, A., Lange, D., Bataille, K. & Hofmann, S., 2006. Interaction between forearc and oceanic plate at the south-central Chilean margin as seen in local seismic data, *Geophys. Res. Lett.,* **33**(23), L23302.

Hackney, R.I. *et al.*, 2006. The segmented plate and coupling at the South-Chilean margin (36–45°S), in *The Andes–Active Subduction Orogeny,* Frontiers in Earth Sciences, pp. 355–374, eds Oucker, O. *et al.,* Springer, Berlin.

Heesemann, M., Grevemeyer, I., Villinger, H., Flueh, E., Scherwath, M., Völker, D., Contreras-Reyes, E. & the TIPTEQ Research Group, 2007. Seaward thermal and structural variability along the rupture area of the 1960 Chile Earthquake and its impact on the seismogenic updip limit, *Geophys. Res. Abstr.,* **9,** 04248.

Hyndman, R.D. & Wang, K., 1993. Thermal constraints on the zone of major thrust earthquake failure-the Cascadia subduction zone, *J. geophys. Res.,* **98**(B2), 2039–2060.

Ivandic, M., Grevemeyer, I., Berhorst, A., Flueh, E.R. & McIntosh, K., 2008. Impact of bending related faulting on the seismic properties of the incoming oceanic plate offshore of Nicaragua, *J. geophys. Res.,* **113,** B05410, doi:10.1029/2007JB005291.

Kapinos, G. & Brasse, H., 2006. A combined on- and offshore magnetotelluric study in South Chile, *Geophys. Res. Abstr.,* **8,** 02199.

Kirby, S., Engdahl, E.R. & Denlinger, R., 1996. Intermediate-depth intraslab earthquakes and arc volcanism as physical expressions of crustal and uppermost mantle metamorphism and subducting slabs, in *Subduction: Top to Bottom,* Vol. 96, pp. 195–214, eds Bebout, G.E., Scholl, D., Kirby, S.H. & Platt, J.P., Geophys. Monograph, Am. Geophys. U.

Krawczyk, C.M. *et al*., 2006. Geophysical sig*nature*s and active tectonics at the south-central Chilean margin, in *The Andes-Active Subduction Orogeny, Frontiers in Earth Sciences,* pp. 171–192, eds Oncken, O. *et al*., Springer, Berlin.

Lange, D., Rietbrock, A., Haberland, C., Bataille, K., Dahm, T., Tilmann, F. & Flueh, E.R., 2007. Seismicity and geometry of the south Chilean subduction zone (41.5 degrees S-43.5 degrees S): implications for controlling parameters, *Geophys. Res. Lett.,* **34**(6), L06311, doi:10.1029/2006GL029190.

Lefeldt, M. & Grevemeyer, I., 2008. Centroid depth and mechanism of trench-outer rise earthquakes, *Geophys. J. Int.,* **172,** 240–251.

Melnick, D. & Echtler, H.P., 2006. Inversion of forearc basins in south-central Chile caused by rapid glacial age trench fill, *Geology,* **34**(9), 709–712, doi:10.1130/G22440.1.

Melnick, D., Bookhagen, B., Echtler, H.P. & Strecker, M.R., 2006. Coastal deformation and great subduction earthquakes, Isla Santa Maria, Chile (37 degrees S), *Geol. Soc. Am. Bull.,* **118**(11–12), 1463–1480.

Mordohovich, C., 1974. Geology of a part of the Pacific margin of Chile, in *The Geology of Continental Margins,* pp. 591–598, eds Burk, C.A. & Drake, C.L., Springer Verlag, New York.

Oleskevich, D.A., Hyndman, R.D. & Wang, K., 1999. The updip and downdip limits to great subduction earthquakes: thermal and structural models of Cascadia, south Alaska, SW Japan, and Chile, *J. geophys. Res.,* **104**(B7), 14 965–14 991.

Ranero, C.R. & Sallares, V., 2004. Geophysical evidence for alteration of the crust and mantle of the Nazca Plate during bending at the north Chile trench, *Geology,* **32,** 549–552.

Ranero, C.R., Morgan, J. Phipps, McIntosh, K. & Reichert, C., 2003. Bending, faulting, and mantle serpentinization at the Middle America trench, *Nature,* **425,** 367–373.

Ranero, C.R., Villasenor, A., Morgan, Phipps, J. & Weinrebe, W., 2005. Relationship between bend-faulting at trenches and intermediate-depth seismicity, *Geochem. Geophys. Geosyst.,* **6,** Q12002, doi:10.1029/2005GC000997.

Ranero, C.R., von Huene, R., Weinrebe, W. & Reichert, C., 2006. Tectonic processes along the Chile convergent margin, in *The Andes-Active Subduction Orogeny, Frontiers in Earth Sciences,* pp. 91–121, eds Oncken, O. *et al*., Springer, Berlin.

Rietbrock, A., Haberland, C., Bataille, K., Dahm, T. & Oncken, O., 2005. Studying the seismogenic coupling zone with a passive seismic array, *Eos Trans. AGU,* **86**(32), 293–300.

Roeser, G., Behrmann, J.H., Kopf, A., 2007. Did differences in strength and frictional behaviour of subducted sediment constrain the rupture of the great 1960 Chile earthquake? *Geophys. Res. Abstr.,* **9,** 05349.

Scherwath, M., Flueh, E., Grevemeyer, I., Tilmann, F., Contreras-Reyes, E. & Weinrebe, W., 2006. Investigating subduction zone processes in Chile, *Eos Trans. AGU,* **87**(27), 265–272.

Scholl, D.W., Kirby, S.H., Keranen, K.M., Wells, R.E., Blakely, R.J., Fisher, M. & von Huene, R., 2007. Megathrust slip and the care and feeding of the subduction channel through which the seismogenic zone runs, *Eos Trans. AGU,* **88**(52), Fall Meet. Suppl., Abstract T51E-06.

Song, T.R.A. & Simons, M., 2003. Large trenchparallel gravity variations predict seismogenic behavior in subduction zones, *Science,* **301,** 630–633, doi:10.1126/science.1085557.

Stein, S. & Stein, C.A., 1996. Thermo-mechanical evolution of oceanic lithosphere: implications for the subduction process and deep eartquakes,

in *Subduction: Top to Bottom,* Vol. 96, pp. 1–17, eds Bebout, G.E., Scholl, D., Kirby, S.H. & Platt, J.P., Geophys. Monograph, Am. Geophys. U.

Takahashi, N., Kodaira, S., Tatsumi, Y., Kaneda, Y. & Suyehiro, K., 2008. Structure and growth of the Izu-Bonin-Mariana arc crust: 1. Seismic constraint on crust and mantle structure of the Mariana arc-back-arc system, *J. geophys. Res.,* **113,** B01104, doi:10.1029/2007JB005120.

Tassara, A., Swain, C., Hackney, R. & Kirby, J., 2007. Elastic thickness structure of South America estimated using wavelets and satellite-derived gravity data, *Earth planet. Sci. Lett.,* **253**(1–2), 17–36.

Taylor, F.W., Briggs, R.W., Frohlich, C., Brown, A., Hornbach, M., Papabatu, A.K., Meltzner, A.J. & Billy, D., 2008. Rupture across arc segment and plate boundaries in the 1 April 2007 Solomons earthquake, *Nat. Geosci.,* **1,** 253–257, doi:10.1038/ngeo159.

Tebbens, S.F., Cande, S.C., Kovacs, L., Parra, J.C., LaBrecque, J.L. & Vergara, H., 1997. The Chile ridge: a tectonic framework, *J. geophys. Res.,* **102**(B6), 12 035–12 060.

Thierer, P.O., Flueh, E.R., Kopp, H., Tilmann, F., Comte, D. & Contreras, S., 2005. Local earthquake monitoring offshore Valparaiso, Chile, *N. Jb. Geol. Paläont. Abh.,* **236**(1/2), 173–183.

Tilmann, F.J., Grevemeyer, I., Flueh, E.R., Dahm, T. & Gossler, J., 2008. Seismicity in the outer rise offshore southern Chile: indication of fluid effects in crust and mantle, *Earth planet. Sci. Lett.,* **269**(1–2), 41–55.

Voelker, D., Wiedicke, M., Ladage, S., Gaedicke, Ch., Reichert, C., Rauch, K., Kramer, W. & Heubeck, C., 2006. Latitudinal variation in sedimentary processes in the Peru-Chile Trench off Central Chile, in *The Andes-Active Subduction Orogeny, Frontiers in Earth Sciences,* pp. 193–216, eds Oncken, O. *et al*., Springer, Berlin.

Voelker, D., Grevemeyer, I., He, J., Wang, K. & Heesemann, M., 2007. Thermal regime of the Chilean Subduction Zone at 38°S and 43°S: modelling results and implications for seismicity, *Geophys. Res. Abstr.,* **9,** 06274.

von Huene, R., Corvalan, J., Flueh, E.R., Hinz, K., Korstgard, J., Ranero, C.R., Weinrebe, W. & the CONDOR Scientists, 1997. Tectonic control of the subducting Juan Fernández Ridge on the Andean margin near Valparaiso, Chile, *Tectonics,* **16,** 474–488.

Weinrebe, W. & Schenk, S., (eds), 2006. RV Meteor Cruise Report M67/1 Chile Margin Survey, IFM-GEOMAR Report No 7, Kiel, Germany, 113 pp.

Wessel, P. & Smith, W.H.S., 1998. New version of generic mapping tools released, *Eos Trans. AGU,* **79,** 579.

White, R.S., McKenzie, D. & O'Nions, R.K., 1992. Oceanic crustal thickness from seismic measurements and rare earth element inversions, *J. geophys. Res.,* **97,** 19 683–19 715.

Yanez, G., Ranero, C.R. & Diaz, J., 2001. Magnetic Anomaly interpretation across the southern central Andes (32°-34°S): the role of the Juan Fernandez Ridge in the late Tertiary evolution of the margin, *J. geophys. Res,* **106**(B4), 6325–6345.

Zelt, C.A., 1999. Modelling strategies and model assessment for wide-angle seismic traveltime data, *Geophys. J. Int.,* **139,** 183–204.

Zelt, C.A. & Forsyth, D.A., 1994. Modeling wide-angle seismic data for crustal structure: southeastern Grenville Province, *J. geophys. Res.,* **99**(B6), 11 687–11 704.

Zelt, C.A. & Smith, R.B., 1992. Seismic traveltime inversion for 2-D crustal velocity structure, *Geophys. J. Int.,* **108,** 16–34.

Zelt, C.A., Sain, K., Naumenko, J.V. & Sawyer, D.S., 2003. Assessment of crustal velocity models using seismic refraction and reflection tomography, *Geophys. J. Int.,* **153,** 609–626.

SUPPORTING INFORMATION

Additional Supporting Information may be found in the online version of this article:

Figure S1. Examples of data fits for TIPTEQ Corridor 4.
Figure S2. Examples of data fits for TIPTEQ Corridor 3.
Figure S3. Examples of data fits for TIPTEQ Corridor 2.

Please note: Wiley-Blackwell are not responsible for the content or functionality of any supporting materials supplied by the authors. Any queries (other than missing material) should be directed to the corresponding author for the article.